

## *Chapter 3*

# METALLIC SOLUTION GROWTH TECHNIQUES

In this chapter we discuss the four solution techniques known as Liquid Phase Epitaxy (LPE), Liquid Phase Electroepitaxy (LPEE), the Traveling Heater method (THM), and Liquid Phase Diffusion (LPD). These crystal growth techniques are briefly introduced, including their descriptions, technical specifications, and technological significances. Some recent experimental studies in each of these techniques are covered in detail. The materials focused on are single crystal *Si* and *SiGe*, and the III-V and II-VI compounds and alloys such as *GaAs*, *GaSb*, *GaInAs*, *GaInSb*, *CdTe*, and *CdZnTe*, etc.. The use of innovative techniques and applied magnetic fields are included. A section on the Epitaxial Lateral Overgrowth (ELO) by LPE is included.

### **3.1. Introduction**

As we have discussed previously, the driving force behind solution growth technologies as they are applied to semiconducting materials lies in their ability to remove the technological limitations for novel device concepts and structures imposed by the small number of available elemental and compound semiconducting substrates, and a limited number of lattice parameters and bandgaps. A slight mismatch between the lattice parameters of a substrate and epitaxial device layer will lead to the creation and propagation of dislocations from the initial growth interface into the device structure, leading to reduced device efficiency and performance. For example, there has been significant interest in the production of high efficiency Laser Diodes (LD's) in the blue

region of the spectrum, to complement the available green and red semiconductor laser diodes for use in color printers, and also for use as blue Light Emitting Diodes (LED's) for the efficient production of white light (although alternative methods are being pursued using Gallium Nitride ( $GaN$ ), and by using suitable mixtures of phosphor coatings to produce multiple emission wavelengths to simulate white light). Zinc Selenide ( $ZnSe$ ) is a suitable candidate material for blue light emission but has a lattice parameter approximately 4% greater than that of the nearest readily available substrate material, Gallium Arsenide ( $GaAs$ ). See, for example, Bevan [1997]. The addition of 4 mole percent of Indium Arsenide ( $InAs$ ) to  $GaAs$  increases the lattice parameter to match that of  $ZnSe$ . The availability of uniform composition substrates lattice matched to  $ZnSe$  would eliminate the propagation of threading dislocations into the device structure (see, for example, Bonner [1988], and Lent [1994a,b]). Similarly, the availability of tunable bandgaps allows the device engineer to tailor the substrate to match a specific region of the spectrum to optimize multi-junction solar cells, for example.

However, as we have discussed previously, the  $GaAs-InAs$  material system exhibits a continuous range of solid solubility with a wide separation between the solidus and liquidus across the entire pseudo-binary phase diagram Wooley and Smith [1957]. Traditional melt growth techniques such as the Czochralski and Bridgman methods are only capable of providing limited quantities of uniform composition material by growth from semi-infinite melts, or by resorting to the complexities of floating crucible or continuous melt replenishment technologies, since the melt would become progressively depleted in one component, resulting in a continuous variation in composition of the solidifying crystal. A further complication for melt growth processes is that a suitable seed crystal is required which is closely lattice- and melting point-matched to that of the desired crystal composition for successful initiation of growth without introducing high defect densities in the crystal. A "bootstrapping" technique has been reported by Bonner et al. [1990] whereby a series of small single crystals of incrementally increasing composition is grown sequentially to provide a series of closely matched seeds for use in the subsequent growth step. This can become a costly and time consuming process, particularly where the desired composition lies far from either end of the pseudo-binary phase diagram, or when relatively small quantities of very high crystalline perfection are required in order to carry out research on the feasibility of a novel device concept. Variants of the solution growth technologies which form the basis of this book are all capable of producing a wide range of constant composition crystals with high crystalline perfection by the appropriate choice of solvent and growth temperature.

An idea of the ranges of composition and bandgap available to the device engineer may be seen by reference to Table 3.3.1, which lists the ranges of lattice parameter and bandgap which may be obtained from a selection of materials systems in the technologically important Group III-V semiconducting

materials, for a variety of electronic and opto-electronic applications such as high frequency Pseudomorphic High Electron Mobility Transistors (PHEMPT's), near to mid-IR emitters and detectors, Thermo Photovoltaic devices (TPV's), solar cells and optical computers.

Similarly, the Group II-VI materials systems find applications in the fields of thermal imaging (based on Mercury Cadmium Telluride epitaxial layers lattice-matched to  $Cd_{0.96}Zn_{0.04}Te$  substrates), for Focal Plane Arrays, and in nuclear medical imaging, High Energy Physics and Astrophysics, based on bulk  $Cd_{0.90}Zn_{0.10}Te$  solid state x- and  $\gamma$ -ray detectors operating at room temperature. The Group IV-IV system *Si-Ge* is also technologically important in the fields of, for example, high electron mobility field effect transistors for high speed computing applications (Cressler [1995]), where the addition of a few atom percent of *Ge* to *Si* increases the electron mobility, and hence the maximum operating frequency for a given device size, to rival that of GaAs-based supercomputers, as photodetectors (Jutzi [2000]) and solar cells (Bremond [1998]). However, the *Si-Ge* phase diagram also exhibits a continuous solid solubility across the entire system (Stöhr [1939]). Alonso [1987] and Stringfellow [1970] used binary data for *Sn* and *Pb*, in a quasichemical equilibrium model, and Malmejac [1972] used a thermodynamic equilibrium model to calculate the phase diagram of the system *Ge-Si-Sb*. For a discussion on the choice of suitable solvent materials for the *Si-Ge* system, see, for example, Stringfellow [1970], Malmejac [1972] and Alonso [1987].

Bulk growth processes for the *Si-Ge* alloy system suffer the same limitations as do the Group III-V and II-VI materials systems. These limitations may also be overcome by solution growth techniques using, for example, the Multicomponent Zone Melting (MCZM) and Liquid Phase Diffusion (LPD) (see the related references in Section 3.5.). An extensive review of the bulk growth of *Si-Ge* solid solutions has been given by Schilz [1995].

Table 3.3.1. Physical Parameters of a selected range of ternary III-V compounds.

Ternary System	Melting Point Range (°C)	Lattice Constant Range (Å)	Bandgap (eV)
<i>InAs-GaAs</i>	943 – 1238	5.654 – 6.058	0.356 – 1.40
<i>InP-GaP</i>	1062 – 1467	5.447 – 5.869	1.35 – 2.24
<i>InAs-InP</i>	943 - 1062	5.869 – 6.058	0.356 – 1.35
<i>GaAs-GaP</i>	1238 – 1467	5.447 – 5.654	1.40 – 2.24
<i>InSb-GaSb</i>	525 – 706	6.095 – 6.497	0.18 – 0.69
<i>InSb-InAs</i>	525 – 943	6.058 – 6.497	1.18 – 0.356

The principal objective of this book is to describe in detail the current state of the art in the numerical simulation and modeling of various growth processes

from metallic solutions, and not to provide an in depth and exhaustive technical description of each process. In order to place the detailed discussions on mathematical simulations in context, and provide the reader with some idea of the experimental background, the growth processes are only briefly discussed, with typical examples by way of illustration only. In this chapter we discuss the four solution techniques of LPE, LPEE, THM and LPD.

### 3.2. Liquid Phase Epitaxy

Liquid Phase Epitaxy (LPE) has been used for many years to grow successive thin layers of various compositions and dopants on semiconductor substrates, to produce active and passive layered structures for a variety of electronic and optoelectronic devices. The most common process involves containing the substrate in a well, machined in a graphite boat, and capped by a graphite slider with a number wells containing different saturated solutions of different compositions and/or dopants, within a horizontal (isothermal) furnace, typically at a temperature around 800-900 °C, depending on the material system and the chosen solvent material. In practice, the slider is positioned such that the first source well is directly over the substrate. Growth of the first layer is initiated by a slow, controlled reduction in temperature, typically 10-20 °C. Re-positioning the slider to bring each saturated solution into alignment over the substrate produces subsequent layers. Details of the sliding boat method may be found in, for example, Logan [1986], Bantien [1987] and Cser [1987] for specific examples.

Alternative procedures have also been used to bring the solvent and substrate in and out of contact. These include tipping (Trah [1990]), rolling about the longitudinal horizontal axis (Bandaru [2001]), and dipping in a vertical furnace configuration (Nelson [1974]), which also includes a discussion of several illustrative LPE-grown devices and applications.

Liquid Phase Epitaxy (LPE) is an extremely versatile growth technique, which has been used to prepare a wide variety of III-V compound and alloy semiconductors. In LPE, supersaturation is usually maintained by gradually lowering the temperature during growth. The reduction in concentration of growth units at the interface gives rise to concentration gradients which provide a driving mechanism for bulk transport in the liquid phase and causes crystallization of the excess solutes onto the substrate. In the growth of III-V binary compounds, the composition of the epitaxial layer is not significantly altered by the change in the solution composition as the growth proceeds due to the near-stoichiometry of the deposit. This is not the case in growth of ternary alloys since the distribution coefficients relating the compositions of the various elements in the solid to their concentrations in the solution may differ from each other. As a consequence the alloy composition may vary significantly as growth proceeds, with a rate of change of alloy composition depending on the initial composition of the solution and the growth temperature. The continuous cooling

and the solute depletion of the solution during LPE growth usually limit the thickness of the layer and sharply grade its composition profile. It is difficult to grow thick epitaxial layers with uniform composition by the conventional LPE method because of depletion of limited solute elements during the growth.

A novel technique for the growth of thick epitaxial layers of  $Si$  and  $Si_{1-x}Ge_x$  by LPE was reported by Sukegawa et al.[1988] and Kimura et al. [1990] (see the pertinent references in Section 5.1), by the so-called *yo-yo solute feeding* method, using  $In$  and  $Sn$  as the solvent. This technique is discussed below since a significant coverage of the LPE modeling presented in Chapter 5 is on this system.

### 3.2.1. LPE Growth in a Sandwich System

In the LPE system developed by Sukegawa et al.[1988] and Kimura et al. [1990] silicon substrates were positioned above and below the solvent, the upper to act as a seed and the lower as a source. A source of  $Si$  replenishment was required, due to segregation effects in the solvent during crystallization onto the seed substrate. By periodically modulating the solvent temperature by 10-20 °C around the average solvent temperature, thick  $Si$  and  $Si_{1-x}Ge_x$  layers were formed on the upper substrate, up to 0.3mm thick  $Si$  layers, and 0.8mm thick  $Si_{1-x}Ge_x$  layers with a value of  $x$  of 0.24. The *yo-yo LPE technique* holds great promise for the growth of high quality material for low-volume applications.

In this technique both growth and dissolution phases are combined in a cyclic

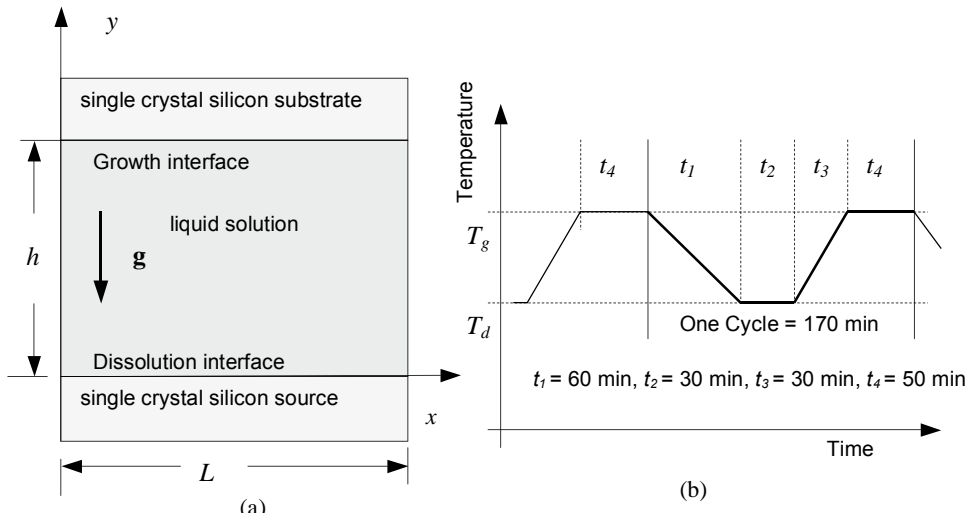


Fig. 3.2.1. (a) Schematic view of the LPE sandwich growth cell, (b) a typical *yo-yo* temperature cycle (for instance  $T_g = 994^\circ\text{C}$  and  $T_d = 974^\circ\text{C}$  for the growth of silicon from an indium solution, redrawn from Sukegawa et al.[1988, 1991b], Kimura et al. [1990]).

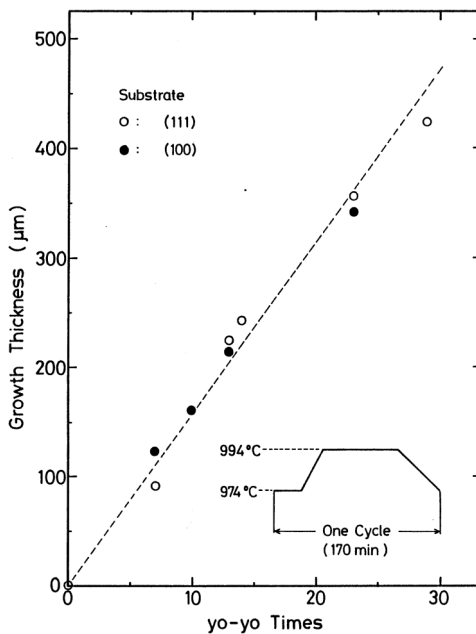


Fig. 3.2.2. Evolution of LPE growth thickness with number of yo-yo cycles (after Sukegawa et al. [1988, 1991b]).

manner. Dissolution occurs mainly on the lower substrate, while growth on the upper substrate is larger than that on the lower substrate. Thus in a cycle, the lower substrate is dissolved to feed the solution which makes it possible to produce thicker epitaxial layers on the upper substrate. This solute feeding method eliminates the difficulty of solute depletion during LPE growth and allows a sustained growth of thick layers with uniform composition (Sukegawa et al. [1991]).

The key feature in the LPE temperature modulation technique is the different transport rates at the upper and lower substrates. These phenomena were attributed to natural convection driven by solutal concentration gradients (Erbay et al. [1993a,b], and Kimura et al. [1994]). In LPE, the mass transfer between the crystal substrate and the surrounding liquid causes a change in the density of the solution which gives rise to natural convection. For sufficiently large solution height, convection enhances mass transport rate in the solution near the upper substrate during growth whereas it increases mass transport rate in the vicinity of the lower substrate during dissolution. The temperature modulation technique relies on the beneficial use of solutal convection. Effective control of convection in LPE growth of bulk crystals is crucial for its success (see Chapter 5 for details).

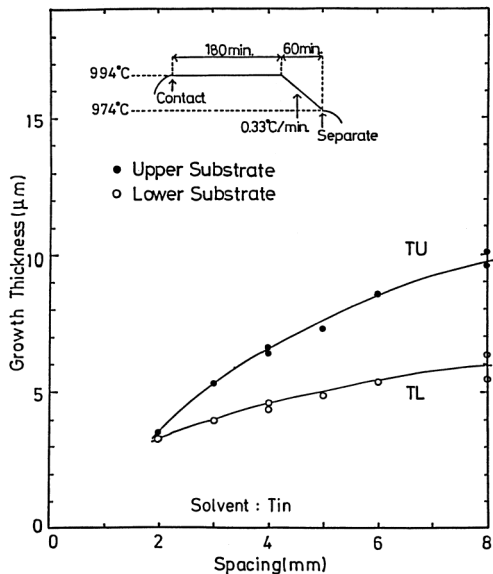


Fig. 3.2.3. Effect of spacing on crystal thickness (after Sukegawa et al. [1990], Kimura et al. [1990]).

A schematic view of the sandwich system developed by Sukagawa et al. [1988, 1991b], and Kimura et al. [1990] is shown in Fig. 3.2.1. The LPE Yo-Yo cycle shown in Fig. 3.2.1 has been applied many times, and successive layers have been grown on the upper substrate. The lower substrate dissolves and supplies the required material to the solution.

The time evolution of the grown silicon layer from an indium solution is shown in Fig. 3.2.2. As seen, between 20 to 30 cycles of growth have been achieved and silicon layers of up to a 400- $\mu\text{m}$  thickness have been grown. This is due to the effect of gravity which raises the convective cells developed in the solution towards the upper substrate. This enhances the growth on the upper substrate, and consequently the growth thickness obtained on the upper substrates is larger than that on the lower substrates. At the same time during the dissolution period (ramping up the temperature) more material dissolves from the lower substrate. This way at the end of each cycle a net growth is achieved at the upper substrate while a net dissolution occurs at the lower substrate.

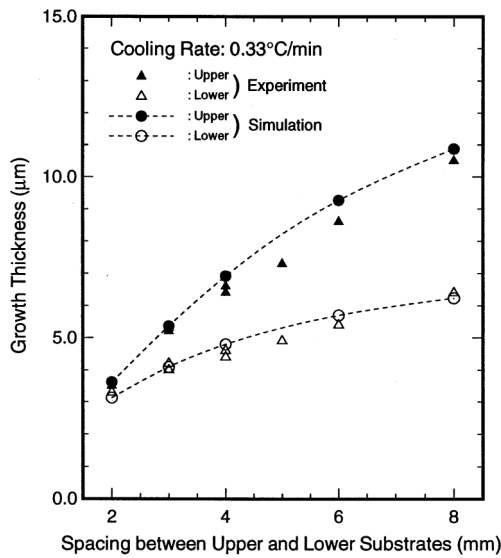


Fig. 3.2.5. Dependence of the average growth thickness on the spacing between the upper and lower substrates (after Kimura et al. [1996a]).

However, the difference in the thicknesses of the upper and lower substrates depends on the spacing between the substrates. For instance, the thicknesses of the grown layers are almost the same for a 2-mm spacing, and increase with increasing spacing. A typical experimental data is shown in Fig. 3.2.3 for the growth of silicon from a tin-solution.

An experimental parametric study has been conducted by Kimura et al. [1994] for the LPE growth of *Si* from a *Sn* solution. The graphite boat used in these experiments is shown in Fig. 3.2.4, and is in the form of a split barrel with a slider. The barrel has a solution chamber, and the solution is contacted with the source silicon crystal during the heating phase to establish an exact

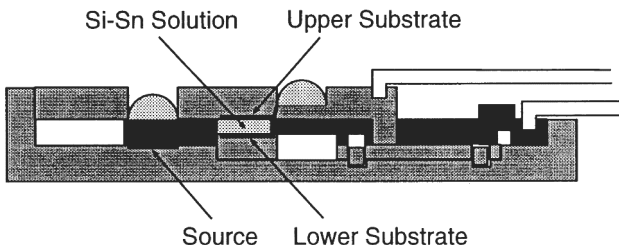


Fig. 3.2.4. Schematic view of the LPE graphite boat used in growth of silicon from a tin solution (after Kimura et al. [1994]).

saturation at the growth temperature. The solution can be brought into contact or removed from the substrates by moving the slider through the barrel (for further details on the experimental apparatus and procedure, see Kanai et al. [1993]).

Ramp cooling growth experiments were performed using (111) oriented  $2 \times 2\text{ cm}^2$ , n-type silicon substrates, and tin as a solvent in a flow of Pd-diffused H<sub>2</sub>. Two substrates were set face to face horizontally in a sandwich configuration in the graphite boat; the gap between substrates (solution height) was varied from 2 to 8 mm. The temperature cycle shown in Fig. 3.2.3 was used. Both substrates and the solution were heated to 994°C and the tin solution, saturated with silicon, was inserted between the two substrates. After a three hours waiting period to ensure good wetting, the temperature was lowered to the final temperature (974°C) at a constant cooling rate of 0.33°C/min. Due to the low cooling rate and the good thermal conductivity of the apparatus, no vertical temperature gradient could be detected across the solution during the cooling process.

The experimental averaged growth thicknesses are shown in Fig. 3.2.5 for various solution heights. For  $h = 2$  mm, the upper substrate is only marginally thicker than the lower one. As expected, as  $h$  increases the difference becomes more pronounced due to enhanced convective mass transport in the upper region. At  $h = 8$  mm, the upper substrate is about 70% larger. The overall agreement between measured and computed growth thicknesses is good and indicates that the model captures the essential physics of the process.

The experimental observations of the LPE growth of Si layers have been

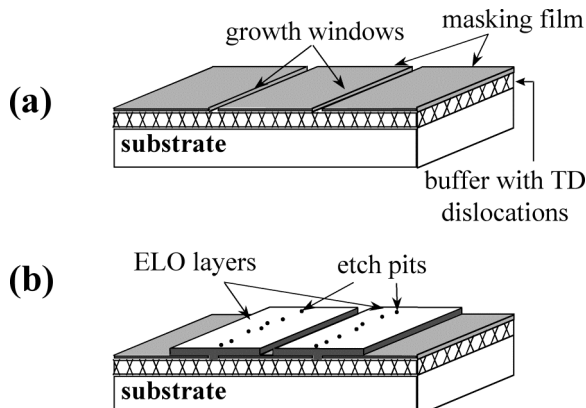


Fig. 3.2.6. Description of the ELO procedure. (a) The growth of relaxed buffer layer is followed by the deposition of an amorphous masking film, the photolithography, and then the etching to open the growth windows. (b) The growth of ELO layers starts selectively from the seeds, and then spread laterally over the mask (after Dobosz and Bryskiewicz [2005]).

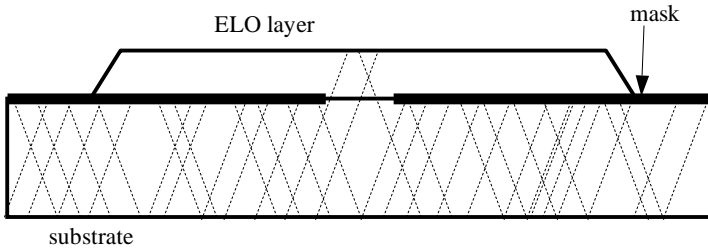


Fig.3.2.7. Propagation of dislocations into the ELO layer through the growth window (dashed-lines represent dislocations), after Zytkiewicz et al, [2005].

modeled through a number of numerical simulations. Details are presented in Chapter 5.

### 3.2.2. Epitaxial Lateral Overgrowth(ELO) of Semiconductors

In this section we briefly cover a new emerging technique of growing high quality, dislocation free thin layers of semiconductors. Today's semiconductor devices require high quality, thin multilayers grown epitaxially on substrates. Defects in the device structure affect the device performance adversely, and lead to faster degradation. Such undesirable defects are very often generated at the substrate/layer interface due to the lattice mismatch between the available substrate and the epitaxial layer. Such defects propagate to the next-grown layer during epitaxy. In order to prevent the propagation of defects, the Epitaxial Lateral Overgrowth (ELO) technique has been developed (here we use the abbreviation of *ELO* for the name of Epitaxial Lateral Overgrowth, see for instance Nishinaga et al. [1988], Ujiie et al. [1989], Nishinaga [1991], Alam et al. [1999], Zytkiewicz [1999], Yan et al. [1998, 1999a,b, 2000], Khenner et al. [2002], Greenspan et al. [2003], and references therein).

ELO is a technique of epitaxial growth on a partially masked-substrate. In ELO, an amorphous mask is deposited on a substrate, and then a narrow line-window structure is created by opening up windows of desired spacing in the mask (Fig.3.2.6a). Epitaxial growth begins in these line windows, and then proceeds in the lateral direction over the mask (Fig.3.2.6b). The lateral growth leads to a new epitaxial layer on the masked substrate, and may fully cover the masked substrate if a sufficient growth time is given for coalescence of adjacent ELO strips (Dobosz and Zytkiewicz [2005]).

Since the mask effectively blocks the propagation of substrate dislocations, laterally overgrown sections of the ELO layers exhibit a much lower dislocation density than that observed in standard planar epilayers grown on the substrate (Fig. 3.2.7). Therefore, when combined with the well-developed methods of buffer layers engineering, the ELO technique offers the possibility of producing high quality substrates with an adjustable value of lattice constant required by modern electronics (see Yan et al. [2000] and Liu et al. [2004]). This is the main

reason for the widespread interest in a deeper understanding of the ELO mechanism and in the development of efficient ELO techniques. Details of the recent ELO modelling studies are presented in Chapter 5.

As examples, Figs. 3.2.8a and 3.2.8b show, respectively, the cross-sections of GaAs (on Si) and GaSb (on GaAs) ELO structures grown by LPE (Dobosz and Bryskiewicz [2006]). The plane views of the same structures after etching are shown in Figs. 3.2.8c and 3.2.8d. In both cases, the density of dislocations found on the top surface of the MBE grown planar buffers was in the range of  $10^8 \text{ cm}^{-2}$ . Since in the ELO process the mask efficiently prevents the propagation of dislocations from the buffer, they thread to the layer through the narrow opening in the mask. As a result, the etch pits on the upper surface are concentrated over the seeding area only, while the laterally overgrown sections exhibit a very lower density of dislocations (see Figs. 3.2.8c and 3.2.8d). These examples clearly show the ability of the ELO technique of blocking threading defects in lattice-mismatched epitaxial structures.

An efficient ELO procedure requires large preferential growth rates (growth anisotropy) in different directions, i.e. the lateral growth of the epilayer is much faster than that in the direction normal to the substrate. By this way, the surface area available for a device application would be the largest. The best way to achieve this goal in the ELO process is to take the advantage of the natural growth anisotropy of various crystal faces (Brice [1973]). On a perfect singular face, atoms can be incorporated into the solid in the form of two-dimensional nuclei only. If the face is singular but imperfect, surface irregularities (e.g. dislocations) supply the steps necessary for its growth. Due to limited rate of surface processes involved, some liquid supersaturation in the vicinity of the liquid/solid interface is required in these two growth modes to achieve a notable growth velocity. On the other hand, atoms can be added to an atomically rough crystal face in a random way and the growth rate of such a face varies linearly with the interface supersaturation.

As discussed by Nishinaga [1991], the basic idea lies in the fundamental dissimilarity between the growth modes of ELO. If a slowly growing facet covers the upper ELO plane whereas the side walls are rough, then at the low supersaturation of the liquid, the growth rates in the vertical and horizontal directions differ significantly and a large anisotropy (a large ELO layer) can be obtained. Usually these conditions are realized using (100) or (111)-oriented substrates. In that case, the optimal orientation of the seeding lines in the substrate plane is determined by the growth of an ELO layer on a masked substrate with a star-like pattern of the seeds. By examining the lateral growth rates with respect to the seed orientation (Dobosz and Zytkiewicz [2005], Zytkiewicz et al. [2005]), it was found that, on (100) GaAs substrates, a large growth anisotropy was obtained when the line seeds were aligned at the angles of  $15^\circ$ ,  $30^\circ$ ,  $60^\circ$  or  $75^\circ$  from the (011) direction (see also Gale et al. [1982], Zhang and Nishinaga [1990], Nishinaga [1991], Naritsuka and Nishinaga [1995], and Zytkiewicz [1999]).

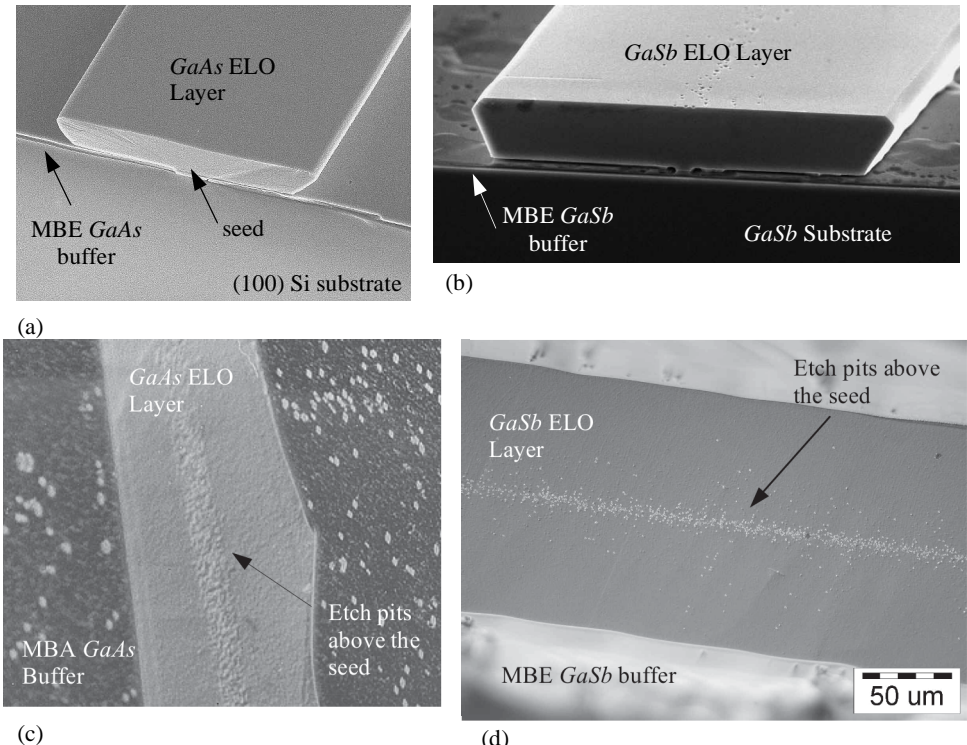


Fig. 3.2.8. Cross-sections of a *GaAs* ELO layer grown on *Si* (a) and a *GaSb* ELO layer grown on *GaAs* (b) by LPE; (c) and (d) show the upper planes of the same samples after selective etching to reveal the distribution of dislocations reaching the ELO surface (after Dubosz and Zytkiewicz [2005]).

Steps on the substrate surface formed due to its off-axis orientation or dislocations enhance the vertical growth of ELO (Nishinaga [1991], Sakawa and Nishinaga [1991], and Zytkiewicz [1999]). Therefore, an additional restriction for the seed direction applies on off-axis orientated substrates. Then, among the many equivalent seed directions that are optimal on the (100) plane, we must choose the one for which the density of misorientation steps inside the seeding area is the smallest (Sakawa and Nishinaga [1991], and Zytkiewicz [1999]). For the same reason, the dislocation density in the buffer must be as low as possible, in order to obtain a ELO layer with a large value of the aspect (width to thickness) ratio (Zytkiewicz [1999]).

Fig. 3.2.9 shows a sketch of an ELO layer grown from a line window on a misoriented substrate. The seeding line direction was assumed to be perpendicular to the substrate miscut direction. In the absence of two-dimensional nucleation, the ELO layer grows by the flow of substrate steps

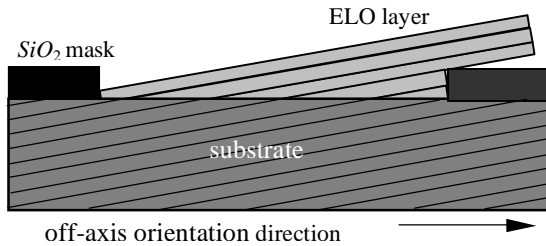


Fig. 3.2.9. Schematic illustration of an ELO growth on an off-axis oriented, dislocation-free substrate; the seeding line is set perpendicular to the substrate off-axis orientation direction (Zytkiewicz et al [2005]).

following the misorientation direction (i.e., to the right). If the substrate misorientation is the only source for surface steps, the ELO growth should stop as soon as all the steps reach the edge of the layer. This means that no growth should take place to the left from the seeding line. Indeed, such a behavior has been observed during the LPE growth of silicon ELO layers on perfect silicon substrates (Bergman [1991]). Actually, a degree of substrate miscut must be applied deliberately to initiate the ELO growth on a defect-free substrate (Bauser [1987], and Bergman [1991]). Otherwise, a larger supersaturation is needed to initiate growth by two-dimensional nucleation, which may lead to the generation of defects in the layer (Bergman [1991]).

Fig. 3.2.10 shows a cross section of the *GaAs* ELO layer grown on a *GaAs* substrate with a surface off-axis oriented by 3° from the (100) plane. The seeds were oriented at 15° from the (0̄1̄1) direction for fast lateral overgrowth, and were nearly perpendicular to the direction of the substrate off-axis orientation. As seen, similar to the previous case, the thickness of the ELO layer is not uniform for the same reason. This time, however, we also observe some growth to the left from the window (i.e. in the direction opposite to the substrate off-axis orientation). Such a growth can be attributed to the dislocations (with a density of  $1.5 \times 10^3 \text{ cm}^{-2}$ ) present in the *GaAs* substrate (Zytkiewicz et al. [2005]). These dislocations provide the required steps to make an additional

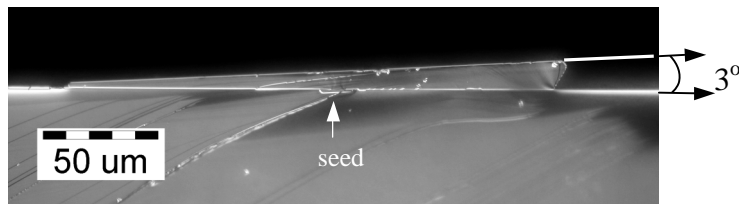


Fig. 3.2.10. A cross section of the *GaAs* ELO layer grown on a *GaAs* substrate with a surface off-axis oriented by 3° from the (100) plane; the substrate is off-axis oriented in the right-hand side direction (Zytkiewicz et al. [2005]).

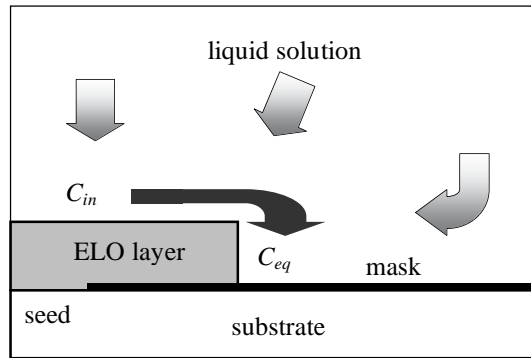


Fig. 3.2.11. A representation of the solute flow during the LPE growth of an ELO layer. The black arrow describes the diffusion of solute in the liquid from the upper surface of ELO to its sidewall (near-surface diffusion) (after Ztykiewicz et al. [2005]).

contribution to the epitaxial growth, allowing a continuous growth of the layer in both directions. The surface of the layer is inclined towards the substrate surface by an angle of  $\approx 3^\circ$  (see Fig. 3.2.10). This is the angle at which the (100) plane intersects with the substrate plane in the (011) cleavage section. This indicates that despite the substrate off-axis orientation, the upper surface of the ELO layer forms the exact (100) plane.

Fig. 3.2.11 describes conceptually the solute movement in the liquid solution occurring during an ELO growth by LPE. Due to symmetry, only half of the substrate and liquid zone is shown. During the LPE growth, the system temperature is slowly lowered to supersaturate the liquid solution. Since there is no nucleation on the mask, the solute species diffuse exclusively towards the seeding area, and are then incorporated into the growing ELO layer. The sidewall of the ELO layer is atomically rough, so there is no barrier for the incorporation of the arriving species into the solid. Therefore, the solute concentration in the liquid zone near the side ELO face is equal to the equilibrium concentration,  $C_{eq}$ , a value that is determined by the phase diagram and actual temperature (see Fig. 5.2.11). However, the upper ELO layer is faceted and the surface solute concentration there,  $C_{in}$ , is larger than the equilibrium concentration. This gives rise to a horizontal solute concentration gradient, and to the so-called near-surface diffusion of solute species from the upper ELO surface to its sidewall (Yan et al. [1999]). It is obvious that the presence of near-surface diffusion enhances the lateral growth of ELO layers.

As mentioned earlier, supersaturation near the crystal faces must be low for a successful ELO growth. Otherwise, two-dimensional nucleation takes place on the upper ELO surface, and leads to a higher vertical growth rate and consequently to a reduced growth anisotropy. In LPE, the surface supersaturation reflects the relative magnitude of the solute supply from the

liquid phase, and the solute consumption at the surface of the growing crystal. Thus, the main parameters controlling these processes are the growth temperature, the initial supercooling of the liquid, and the cooling rate.

The growth anisotropy in ELO depends on the growth temperature (Cheng et al. [1997], Nishinaga [1991], Dobosz and Ztykiewicz [2005], Ztykiewicz et al. [2005]). For high LPE temperatures, the vertical ELO growth rate is usually high since the surface kinetics are very fast. This results in ELO layers with a small value of aspect ratio. Then, the width-to-thickness ratio increases progressively as the growth temperature decreases. Thus, there is an optimum growth temperature  $T_{opt}$  at which ELO layers have the largest value of aspect ratio. As shown by Yan et al. [1999] for *InP* ELO layers,  $T_{opt}$  corresponds to the temperature at which interface supersaturation is the smallest. It is obvious that the optimum ELO growth temperature depends on many parameters such as the slope of the liquidus curve, geometry of the LPE system, etc., so it must be determined experimentally for each particular case under study. Optimum temperature values of 500 °C, 580 °C and 530 °C have been reported for the LPE growth of *InP/InP* (Yan et al. [1999]), *GaAs/GaAs* (Dobosz and Ztykiewicz

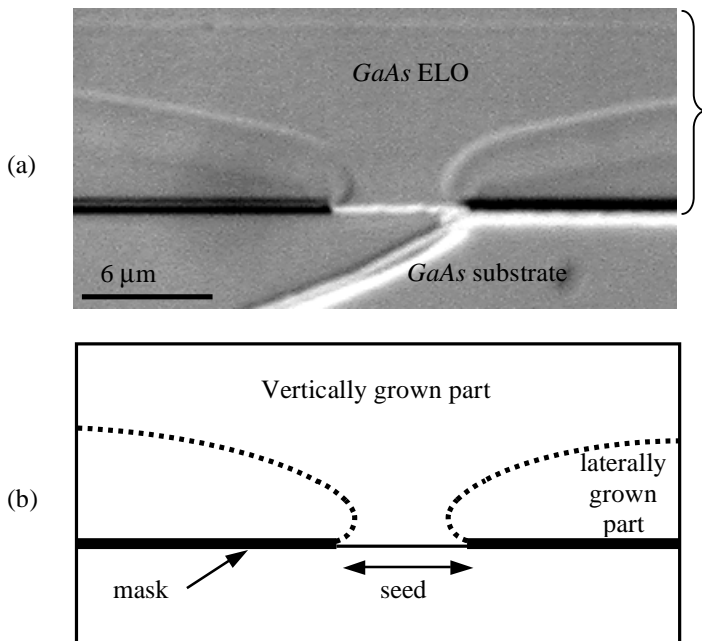


Fig. 3.2.12. A microphotograph (a) and a schematic view (b) of the cross-section of a *Si*-doped *GaAs* ELO layer grown on *GaAs* by LPE without any initial supersaturation; the boundaries between the vertically and laterally grown parts of the layer are marked by dotted line in (b); note the dissolution in the lateral direction caused by the Gibbs-Thomson effect at the beginning of growth (Ztykiewicz et al. [2005]).

[2005]), and *GaAs/Si* (Cheng et al. [1997]) ELO systems, respectively.

To keep the surface supersaturation at a low value, the cooling rate should be as low as possible. This has been observed experimentally for the LPE growth of GaAs (Dobosz and Ztykiewicz [2005]), *InP* (Yan et al. [2000]), and GaSb (Dobosz et al. [2002]) ELO structures. The reason for this is to supply solute to the surface of the growing layer slow enough, so that the solute can be redistributed by near-surface diffusion between the upper and side walls of the ELO cell, and be incorporated into the solid without any increase in the surface supersaturation.

The optimal choice of the initial supercooling during the ELO growth by LPE requires some additional factors to be taken into account. It is apparent that supercooling of the solution should be as low as possible. Then, the initial supersaturation of the solution, and consequently that at the ELO surface, can be kept low. Indeed, experiments show that for the LPE growth of *GaSb* ELO structures, a smaller initial melt supercooling leads to a larger aspect ratio (Dobosz et al. [2002]). Some ELO systems, however, require some initial supercooling of the solution to initiate growth. This is the case for the LPE growth of *Si* ELO layers on defect-free silicon substrates. As shown in Fig. 3.2.9, in such a case the ELO layer grows only by the flow of steps supplied by the substrate off-axis orientation. The sidewall of the layer beginning to grow laterally is strongly curved, and due to the Gibbs-Thomson effect, it requires a higher equilibrium solute concentration than the planar face. Thus, instead of growing laterally the layer is dissolved and cannot emerge through the opening in the mask as long as the liquid solution is not supersaturated sufficiently (Raidt et al. [1996]). The situation is different, however, if dislocations are present in the substrate, enhancing the vertical ELO growth. This point is illustrated in Fig. 3.2.12a by showing a cross-section of the silicon-doped *GaAs* ELO layer grown on a *GaAs* substrate by LPE without any initial supersaturation. The boundaries between the vertically and laterally grown parts of the layer can be revealed by appropriate etching (Ztykiewicz et al. [1999]). These boundaries are sketched in Fig. 3.2.12b by dotted lines. Note that the Gibbs-Thomson effect that induced dissolution in the lateral direction instead of growth is clearly visible at the beginning of epitaxy. However, during the continuous cooling of the system steps supplied by the substrate dislocations still allow for a vertical growth of the layer in the middle of the seed despite a slow dissolution induced by the Gibbs-Thomson effect taking place in the direction parallel to the substrate. As soon as the layer grows thicker, the contribution of the Gibbs-Thomson effect decreases and lateral overgrowth along the mask begins. This example shows again the important role of dislocations in the growth of ELO layers.

### 3.3. Liquid Phase Electroepitaxy

Liquid Phase Electroepitaxy (LPEE) is one of the solution growth techniques by which layers of single crystals are grown at relatively low temperatures. It is a relatively new, promising technique for producing high quality, thick crystals of compound and alloy semiconductors. The LPEE growth technique has been developed during the use of electric current for dopant modulation in LPE (Kumagawa et al. [1973]), and became a solution growth technique for growth of binary and ternary semiconductor crystals (see for instance Daniele et al. [1975], Daniele [1977], Gevorkyan, et al. [1977a,b], Jastrzebski et al. [1976, 1978a,b], and others. The literature on LPEE is relatively rich; we believe that the reference list provided at the end of this book is relatively comprehensive, considering the intention of this book).

Growth in LPEE is initiated and sustained by passing an electric current through the substrate-solution-source system while the overall furnace temperature is kept constant. Since growth takes place at a constant furnace temperature, LPEE has a number of advantages such as, steady and controlled growth rate, controlled doping, improved surface morphology and defect structure, low dislocation density and improved electronic characteristics. In addition, the method is suitable for growing ternary and quaternary alloy crystals with desired compositions. This feature of the technique has attracted interest in the growth of high quality semiconductor crystals since the availability of such thick alloy substrates may solve the problems arising from lattice mismatch encountered in the integration of different material layers. The availability of such thick substrates may open new horizons in the fabrication technology of opto-electronic devices and integrated circuits (OEICs). Due to the technological importance of LPEE, a number of modelling studies have been carried out in recent years (see Chapter 6).

#### 3.3.1. Alloy Semiconductor Substrates

Alloy semiconductors, such as *GaInAs*, *GaInSb*, *GaInP*, and *CdZnTe*, grown on commercially available *GaAs*, *GaSb*, *GaP*, and *CdTe* substrates, are of interest as lattice-matched substrates for novel semiconductor devices in optoelectronics (for detailed information the reader is referred to the source of this section, Bryskiewicz and Laferriere [1993], Bryskiewicz [1994]). For instance,  $Ga_{0.47}In_{0.53}As$  ternary alloy grown epitaxially on the lattice matched *InP* substrate has been used as active layer in lasers and photodetectors in optical communication systems (Lo et al. [1992], Hong et al. [1992]). It is a very good candidate for high-speed transistors because of its high carrier mobility. *GaInAs* epitaxial layers grown on *GaAs* substrates have also been used for High Electron Mobility Transistors (HEMT) structures with significantly improved performance, and for strained-layer lasers, modulators, and detectors operating in the near infrared region (Scharf et al. [1991]). For

this ternary material, however, only thin layers can be grown due to the lattice mismatch. As a result, many problems have been observed in lasers fabricated on such substrates, and are restricted to the 0.8-1.1  $\mu\text{m}$  region (Eastman [1991]).

High performance semiconductor lasers operating in the 2-5  $\mu\text{m}$  range are highly desirable in optical fiber communication systems employing low-loss fluoride-based fibers, laser radar, remote sensing of atmospheric gases, and molecular spectroscopy (Andaspaeva et al. [1988], Choi and Eglash [1991], Eglash and Choi [1992]). However, currently available alloy layers exhibit a miscibility gap in the range of 2.4-4  $\mu\text{m}$  (Choi and Eglash [1991], Eglash and Choi [1992]). The availability of *InAsP*, *GaInAs* and *GaInSb* substrates with desired thicknesses and quality would overcome this difficulty. These materials and many other desired alloy semiconductors either cannot be grown commercially, or are grown with inadequate thickness and quality, or cannot be grown reproducibly. LPEE has proven to have the potential for growing such crystals with the desired properties.

One can conclude that the number of novel, high performance optoelectronic and microwave devices would increase significantly should high quality alloy substrates be available commercially. The alloy materials that can be grown by LPEE are summarized in Table 3.3.1.

Table 3.3.1. Potential applications of alloy semiconductors (Bryskiewicz [1994]).

Semiconductor alloy	Applications
$Ga_{0.96}In_{0.04}As$	substrates lattice matched to blue diodes and lasers ( <i>ZnSe</i> )
$Ga_xIn_{1-x}As$ , $InAs_{1-x}P_x$	substrates suitable for OEICs operating in the 1.3-2 $\mu\text{m}$ region
$Ga_xIn_{1-x}P$ , $GaAs_{1-x}P_x$ $Al_xGa_{1-x}As$	substrates diodes and lasers operating in the visible range
$Hg_{1-x}Cd_xTe$ , $Ga_{1-x}In_xSb$ , $InAs_xSb_{1-x}$	substrates for mid- and far-infrared detectors and lasers
$Si_{1-x}Ge_x$	substrates for n-channel Field Effect Transistors (FETs) and efficient optoelectronic devices, solar cells, photo-detectors
$Cd_xZn_{1-x}Te$	substrates for $\gamma$ - and x-ray detectors,

Semiconductors grown by LPEE show advantages over crystals grown by the melt growth techniques, namely, lack of detectable electron traps (Bryskiewicz et al. [1987a]), low vacancy densities (Dannefear et al. [1978]), low dislocation densities (Boucher et al. [1987]), and high luminescence efficiency (Bryskiewicz et al. [1987b]). The distinct feature of the LPEE growth process is the strong stabilizing effect of the applied electric current on the crystal composition. For example, the mm-thick ingots of *GaInAs* (Bryskiewicz et al. [1987b, 1995, 1988], Sheibani et al. [2003a,b]), *AlGaSb* (Bischopink et al.

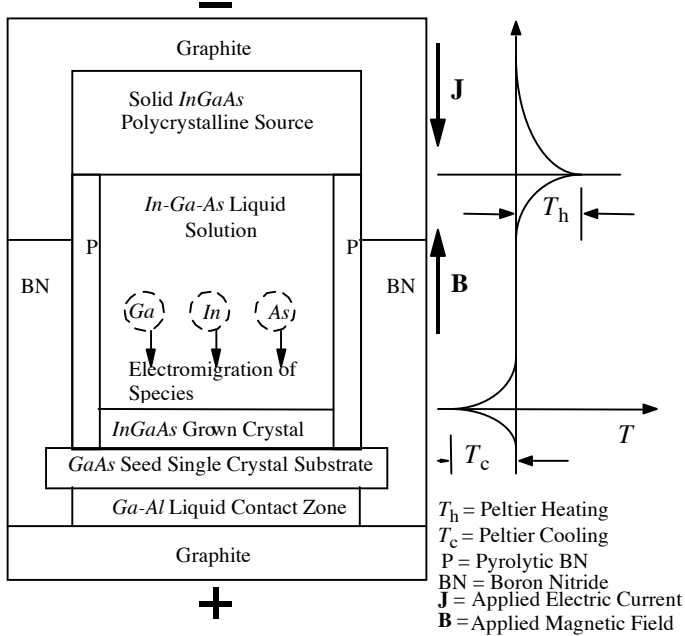


Fig. 3.3.1. A schematic view of an LPEE crucible for a *GaInAs* system. Note that the temperature distribution shown is not the actual one; it describes symbolically the Peltier cooling and Peltier heating at the interfaces.

[1993]) and *AlGaAs* (Danielle and Hebling [1981], Ztykiewicz [1992, 1993, 1995]) exhibit a remarkable compositional uniformity.

The above mentioned features along with its low hardware cost make LPEE quite attractive for the growth of high-quality alloy semiconductors in the form of both bulk crystals and buffer layers. However, a reproducible growth of such crystals requires a good understanding and control of the key mechanisms governing this process. Among these factors, both the gravity induced natural convection and the composition variations in the solution are of the utmost importance. They have adverse effects on the quality of grown crystals and the stability of the growth interface.

### 3.3.2. Liquid Phase Electroepitaxy

In a typical LPEE growth system, graphite electrodes are placed at the top and bottom of the growth cell (Fig. 3.3.1). The substrate is placed at the bottom of the solution and the source material is placed between the solution and the upper electrode. The liquid contact zone located below the substrate provides a uniform, low resistance electrical contact between the lower face of the substrate and the lower electrode, which is essential for satisfactory growth. The

boron-nitride jacket around the horizontal sandwich layers forms the cell and acts both as a heat conductor and as an electrical insulator.

The growth temperature is typically in the range of 650°C-900°C, depending on the material to be grown. After the system reaches thermodynamic equilibrium, the electric current is turned on and growth is initiated. During the growth process, the furnace temperature is kept constant. The applied electric current is the sole external driving force and the controlling element of the growth, and makes it possible to achieve a high growth rate and precise control of the process. The electric current passes through the lower electrode, contact zone, and substrate, but may bypass the source material into the upper electrode as seen in Fig. 3.3.1. A static magnetic field may also be used in LPEE.

We discuss below some of the factors playing role in the LPEE growth process.

### *Thermoelectric Effects*

In a well-designed LPEE apparatus, vertical and horizontal external temperature gradients are effectively minimized. Thermal effects that may lead to temperature gradients in the solution may then be assumed to be solely due to Peltier cooling/heating and Joule heating.

*Peltier cooling/heating* is a thermoelectric effect caused by the electric current passing across the solution-substrate (growth interface) and the substrate-contact zone interfaces. The electric current causes heat absorption or heat evolution at the interfaces, depending on the direction of the electric current. In an equilibrated LPEE system with a positive polarity of the lower electrode, Peltier cooling occurs at the growth interface and is accompanied by Peltier heating at the substrate-contact zone interface. Thus, heat transport across the substrate affects the amount of cooling at the growth interface. Indeed, the amount of cooling at the growth interface increases with increasing substrate thickness. If the current passes through the solution-source (dissolution) interface, Peltier heating occurs at this interface.

Being a semiconductor, the substrate has a high electrical resistivity. The electric current passing through the substrate induces Joule heating proportional to the square of current density and electrical resistivity (Joule heating produced in the solution and graphite electrodes is at least an order of magnitude lower because of the low electrical resistivity). The effect of Joule heating in the substrate increases with the increasing substrate thickness and becomes significant for bulk crystals. A one-dimensional model presented by Ztykiewicz [1996] suggests that the Joule heating may present itself as a thermal limiting factor (barrier) in the growth of very thick crystals. However, this may need to be proven experimentally, or through numerical simulations.

### *Growth Mechanisms*

The main growth mechanism of LPEE is the transport mechanism known as *electromigration*. In the growth of compound and alloy semiconductors, the

solutions are metallic conductors. In such solutions, electromigration takes place due to electron-momentum exchange and electrostatic field forces (Jastrzebski et al. [1976], Bryskiewicz [1978]). Under the influence of the electric field induced by the applied electric current, solute species migrate towards the anode with a velocity proportional to solute mobility and electric field. Thus, when the substrate has a positive polarity, the solution becomes supersaturated with solute near the substrate-solution interface, resulting in epitaxial growth.

The combined effect of Peltier cooling/heating and Joule heating results in an axial temperature gradient. This temperature gradient induces supersaturation of the solution in the vicinity of the growth interface, leading to a further contribution to epitaxial growth. This is the second main growth mechanism in LPEE.

Either electromigration or Peltier cooling can become dominant, depending on the particular growth conditions (Jastrzebski et al. [1978], Takenaka and Nakajima [1991]). However, these contributions can be affected by the presence of natural convection in the solutions as shown numerically by Djilali et al. [1995].

A typical growth rate in LPEE growth of *GaAs* at a  $3 \text{ A/cm}^2$  electric current density is about 0.5 mm/day. For the growth of thick crystals (several millimeters), mass transport in the liquid solution is mainly due to electromigration. The contribution of molecular diffusion is very small, as shown experimentally by Sheibani et al. [2003a,b], and also numerically by Liu et al. [2002, 2004]. The growth rate increases with increasing electric density. However, at higher electric densities, for instance  $10 \text{ A/cm}^2$  or higher, the growth becomes unstable (Sheibani et al. [2003a,b]).

### Natural Convection

The effect of convection has been observed in various experiments (Wilcox [1983], Ostrach [1983], Sheibani et al. [2003a,b]). It enhances the overall transport processes, and thus increases the growth rate, which is desirable. However, convection often has an adverse influence on growth kinetics, and on the structure and quality of grown crystals (Wilcox [1983]). It has been observed that convective flow, resulting from both thermal and solutal gradients, leads to the growth of *GaAs/GaInAs* layers with non-uniform thickness profiles (Jastrzebski et al. [1978], Sheibani et al. [2003a,b]). Furthermore, convection has been found to limit the maximum achievable thickness in bulk crystal growth experiments (Bryskiewicz et al. [1987]), due to a deterioration in the surface quality caused by unstable growth conditions (Sheibani [2003a,b]).

In the growth of alloy semiconductors, convection adds another dimension to the difficulty of the problem. In most alloys, densities of the components are significantly different. This difference in the presence of the gravitational field of Earth gives rise to inhomogeneity in the composition of the liquid solution

during growth. In other words, gravity makes it difficult to maintain the solution with a uniform liquid composition. Less dense component(s) moving upwards leads to depletion of the required component(s) in the vicinity of the growth interface, leading to unsatisfactory growth. For example, in the case of *GaInP*, phosphorus, with the smallest density, tends to float.

### *Applied Magnetic Fields*

In order to suppress convection, a static, external applied magnetic field is also used in LPEE growth of crystals (Sheibani et al. [2003a,b]). As we will see later, the application of a vertical static magnetic field (perfectly aligned with the growth direction and the applied electric field) indeed suppresses convection significantly. However, it was also observed, unexpectedly though, that the applied magnetic field increases growth rate very significantly. For instance, a field of 4.5 kG increases the growth rate about ten fold. Experimental (Sheibani et al. [2003a,b]) and modeling (Dost et al. [2002, 2003, 2004], Liu et al. [2002a,b, 2003, 2004]) studies have shown that the growth rate is also proportional to the intensity of the applied magnetic field; however its contribution to mass transport is about twice that of the applied electric current.

The literature on the experimental studies carried out for the LPEE growth various semiconductors is relatively rich. Most of the fundamental aspects of the LPEE growth process are covered in Chapter 6. In the next section, due to its significance, we present a recent experimental study of Sheibani et al. [2003a] that has been carried out for the LPEE growth of *GaInAs* under a strong static magnetic field.

#### *3.3.3. LPEE Growth of GaInAs Under a Stationary Magnetic Field*

As mentioned earlier, in spite of many significant advantages, LPEE has thus far suffered from mainly three *shortfalls* towards its commercialization. The first is the achievable crystal thickness that is relatively small, in the order of a few millimeters. This is mainly due to the combined effect of Peltier and Joule heating in the system, leading to higher temperature gradients and a relatively strong natural convection in the liquid solution zone that cause unsatisfactory and unstable growth. This puts a limit on the achievable crystal thickness, particularly in the growth of bulk crystals, and providing less useful material. The second shortfall of LPEE has been its low growth rate. The growth rate in LPEE is almost linearly proportional with the applied electric current, and is about 0.5 mm/day at a 3 A/cm<sup>2</sup> electric current density. Of course, for higher electric current density levels, the growth rate will increase, but in the growth of thick (bulk) crystals the combined effect of temperature gradients and natural convection will lead to an unstable growth. The third shortfall is the need for a single crystal seed of the same composition as the crystal to be grown. Small compositional differences, in the order of 4% depending on the crystal lattice

parameters, can be tolerated, but higher compositional differences may lead to unsatisfactory growth.

The first two shortfalls of LPEE have recently been addressed by Sheibani et al. [2003a]. By optimizing the growth parameters of LPEE, and also by using a static external applied magnetic field, a number of bulk (thick), flat *GaAs* crystals and  $In_{0.04}Ga_{0.96}As$  single crystals of uniform compositions were grown, and the growth rate of LPEE was increased more than 10 times for a selected electric current density. The grown crystals under magnetic field or no magnetic field were all single crystals, and the results were reproducible in terms of crystal thickness, growth rate, and compositional uniformity. The addressing of the third shortfall of LPEE has been attempted by utilizing the Liquid Phase Diffusion (LPD) technique (see Section 3.5).

A comprehensive experimental study of the LPEE growth of *GaAs* and  $Ga_{0.96}In_{0.04}As$  single crystals has been carried using the facility in the Crystal Growth Laboratory (CGL) of the University of Victoria. The LPEE experiments under no magnetic field have lead to the growth of a large number of *GaAs* and  $Ga_{0.96}In_{0.04}As$  single crystals of thicknesses up to 9 mm. It was possible to be able to apply electric current densities of 3, 5, and 7 A/cm<sup>2</sup>. The corresponding growth rates in these experiments were about 0.57, 0.75 and 1.25 mm/day, respectively. Growth interfaces were very flat, and the growth experiments were reproducible in terms of crystal thickness and growth rate. Experiments at higher electric current intensities were not successful.

Experiments at 3, 5 and 7 A/cm<sup>2</sup> electric current densities were repeated under various applied static magnetic field levels, starting at 3 A/cm<sup>2</sup> electric current density and 20 kG magnetic field level (based on an earlier initial numerical estimation of Qin and Dost [1996]). The LPEE experiments at the 4.5 kG and lower magnetic field levels were successful, but those under higher magnetic field levels were not. These experiments indicate that for the LPEE system used in Sheibani et al. [2003a] the 4.5 kG field level is the maximum field intensity (*critical*) above which the growth is not stable. The numerical simulations conducted under the same condition yield a lower *critical* magnetic field level, which is about 2.0-3.0 kG (Liu et al. [2002]). In addition, the experimental LPEE growth rates under magnetic field are much higher than those under no magnetic field. For instance, as we will see later, the growth at 4.5 kG magnetic field level was about 10 times higher than that under no magnetic field (at  $J = 3$  A/cm<sup>2</sup>). The experiments performed at the  $B = 1.0$  and 2.0 kG field levels (at  $J = 3$  A/cm<sup>2</sup>) were also successful, and the growth rates were also higher at 1.62 and 2.35 mm/day, respectively. Experiments showed that the application of an external magnetic field is very beneficial in increasing the growth rate in LPEE to a competitive level with other bulk crystal growth techniques.

At the higher magnetic field levels (even at the  $J = 3$  A/cm<sup>2</sup> electric current density level), and the higher electric current density levels ( $J = 10$  A/cm<sup>2</sup> or higher), the experiments did not lead to a successful growth, but showed very

interesting outcomes. Although very thick crystals were grown, even up to a 9 mm thickness, the growth processes were not stable and led to unevenly grown crystals. From the visual inspection of the grown crystals, the adverse effect of natural convection was obvious causing either one sided growth or particularly in four experiments, leading to holes in the grown crystals. It was considered that such a growth (one-sided and with holes) is because of the strong and unstable convection in the liquid zones (solution and contact zones) due to the strong interaction between the magnetic field and the applied electric current. Such predictions were confirmed qualitatively by numerical simulations (see Chapter 6 for details).

### *The LPEE System for the Growth of GaInAs*

A schematic view of the LPEE growth system used at the University of Victoria is shown in Fig. 3.3.2. A view of the CGL growth room is also shown in Fig. 3.3.3. Some of the related system parameters, and the measured furnace temperature profile are given in Table 3.3.2. The first element in the apparatus consists of a crucible in which the substrate, the solution, and the source material are contained. The crucible is held within a quartz reactor tube by four molybdenum rods, two of which act as electrodes. High purity hydrogen flows through the reactor tube during growth. At one end, the reactor tube is constrained by a vacuum-tight sealed flange, through which electrodes are inserted. These electrodes reach the crucible, and allow the DC current from a power supply to flow through the growth cell within the crucible. A thermocouple is also inserted through the flange, and extends up to the crucible. The direct electric current needed to sustain the growth is provided by a 100A,

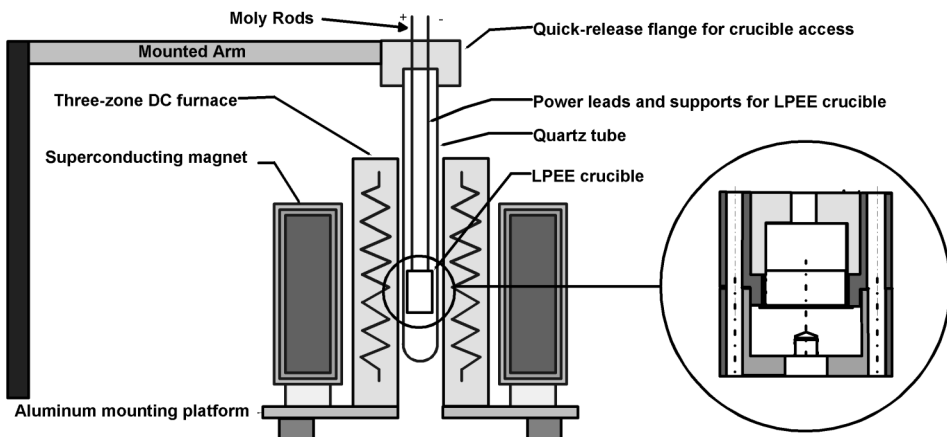


Fig. 3.3.2. A schematic view of the LPEE growth system used at CGL at the University of Victoria (after Sheibani et al. [2003a]).

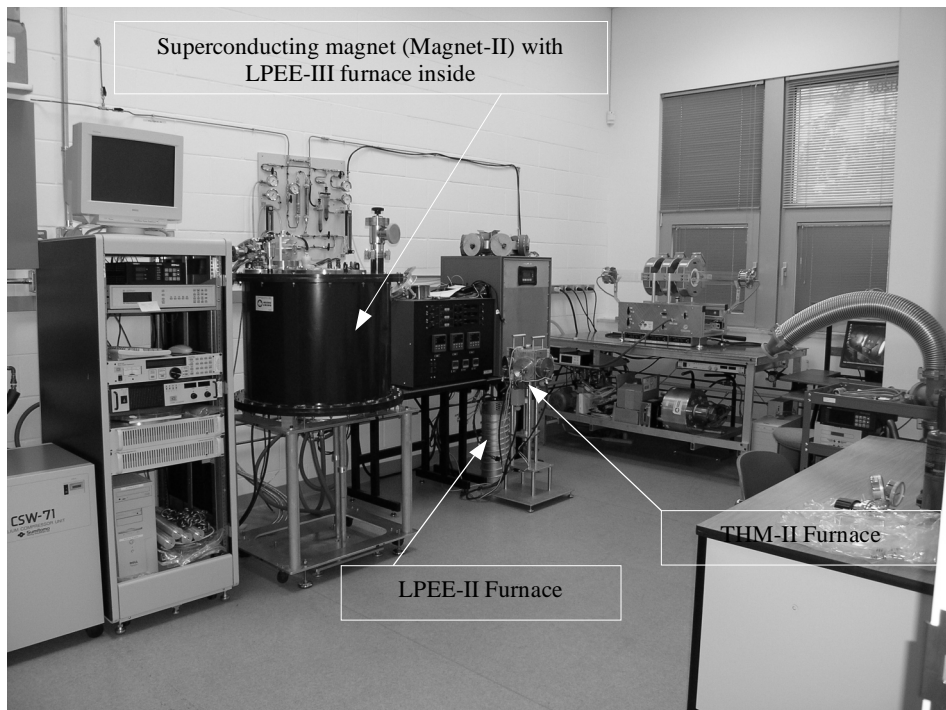


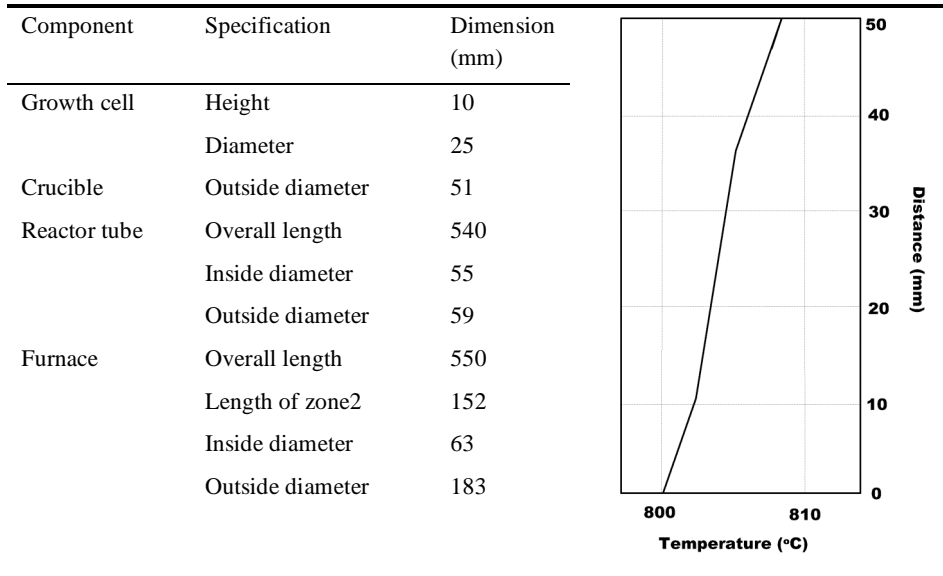
Fig. 3.3.3. A view of CGL Growth Room-II. Magnet-II and LPEE-III furnace are seen on the left. Magnet-II is a magnetically-cooled superconducting magnet. LPEE furnaces were built using non-magnetizable materials.

10V power supply. The reactor tube sits inside a three-zone furnace with independent temperature controllers. The furnace and magnet rest on an aluminum platform that can be adjusted by means of leveling screws. The reactor and end flange are fixed on a horizontal aluminum arm. This arm is mounted on the wall to prevent the crucible from being subjected to the vibration generated by the magnet.

The polycrystalline source material in the crucible is placed above the liquid solution, and the solution sits on the single crystal seed substrate. To ensure a uniform electric current distribution throughout the seed crystal during growth, a liquid contact zone (a gallium-rich aluminum alloy is inserted below the seed, between the seed and the lower graphite. The growth liquid solution is prepared outside, and then inserted into the growth cell. The furnace is then heated to the growth temperature in the range of 780-900°C. After a waiting period of time to allow the system to reach the thermodynamic equilibrium, the electric current is turned on and the growth is initiated. During growth, the furnace temperature is kept constant. The applied electric current passing through the growth cell is the sole driving force for growth. During the experiments conducted under

magnetic field, the system was also subjected to a static, vertical external magnetic field.

Table 3.3.2. System dimensions, and the measured temperature profile (Sheibani et al. [2003a]).



The growth crucible is the most critical part of the LPEE crystal growth system, and a number of features were kept in mind in its design. The crucible was designed to: i) provide electrical insulation between the two electrodes, except through the solution-substrate interfaces, ii) allow for thermal expansion of its components, iii) provide uniform electrical contact at the back of the seed substrate, iv) prevent solution leak, v) minimize the amount of impurities released from the crucible into the solution, vi) allow easy removal of materials at the end of the growth experiment, vii) be able to be reusable, and viii) allow the insertion of a system for temperature monitoring within the crucible.

During growth, hydrogen is constantly flowed through the reactor tube to prevent the accumulation of impurities. Between the hydrogen supply cylinder and the reactor tube, the hydrogen is first purified to lower the amount of impurities in the stream to under 10 ppb levels, and then filtered to remove unwanted particles. Hydrogen enters the reactor tube through the end flange and exits at the outlet. A turbomolecular pump is also connected to the reactor via the same end flange.

#### *Growth Procedure*

The charge materials with high purity (4N-6N), i.e., *Ga*, *In*, *GaAs*, and *Al* (used for the liquid solution and contact zones), and the source *GaInAs* are

etched by chemical solutions before loading them into the crucible. *Ga* and *Al* are prepared for the liquid contact zone and etched by  $HCl/H_2O = 1/9$  and  $H_3PO_4/H_2O = 1/2$  respectively. They are placed at the bottom cavity between the graphite base and the substrate. The weight ratio of the contact liquid is selected as 31w%-*Al*. A one-face-polished *GaAs* (100) substrate of 0.5-1.3 mm thickness and 27x27 mm dimensions is etched by a solution of  $H_2SO_4/H_2O_2/H_2O = 4/1/1$  and 48%-*HF*, and is then placed on the *BN* (boron nitride) substrate holder. In order to ensure perfectly uniform electric current passage, the substrate should be in complete contact with the alloy contact liquid. Poly-crystalline *GaAs* or *GaInAs* source material is etched by the same chemical solution, and then placed above the upper graphite section of the crucible. Then, *Ga* pellets, *In* shot, and *GaAs* chips are prepared for the liquid solution. The etching processes of *Ga* and *In* are the same as that for *Ga* used in the contact zone, and *GaAs* is etched by the same chemical solution used for the substrate. The weight-ratio of *Ga* pellets and *GaAs* chips is determined from the phase diagram about 800°C, which is the selected growth temperature in the LPEE experiments. The solution materials are then placed in the upper section of the graphite container of the crucible before initiating the growth process.

The growth crucible components are then assembled, and placed into the quartz tube. The quartz tube is inserted into its selected position in the three-zone furnace. The furnace temperature profile is set to a certain temperature profile that was determined by temperature profiling using a dummy system (Table 3.3.2). Two electrodes are inserted, ensuring that they reach the crucible in order to allow the electric current flow through the growth cell. The positive and negative electrodes are connected respectively to the bottom and upper graphite sections. K-type thermocouples are also inserted to monitor the furnace temperature. After the tube is completely purged by hydrogen gas, hydrogen is flowed through the tube during the growth with 30-40 ml/min and pressure in the tube is controlled about 1.5atm. At first, the furnace temperature is raised up to 450°C and held for 1 hr to obtain the stable alloy-melt in the contact zone, and then raised again up to about 800°C (growth temperature). The temperature gradient along the growth cell must be less than 0.5° C/mm as shown in Table 3.3.2. The electric current is turned on and the growth is initiated after a carbon plug is pulled up to supply the solution to the growth zone. At the end of the growth period, the electric current and furnace power are turned off and the system is allowed to cool to room temperature.

### Experimental Results

This section presents the experimental results of the LPEE growth of *GaAs* and *InGaAs*. Most of the growth parameters necessary for the successful operation of the growth setup were determined by growing *GaAs* first, before attempting the growth of the ternary alloy  $In_{0.04}Ga_{0.96}As$  (with a 4% *In*-content).

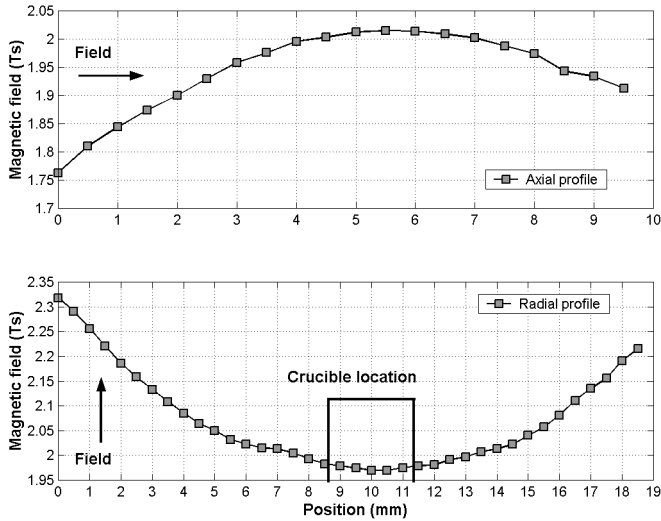


Fig. 3.3.4. The static magnetic field distribution in the opening of the superconducting magnet (Magnet-I) of CGL (after Sheibani et al. [2003a]).

The main reason for such an approach was due to the fact that we wanted first to improve the growth technique and its procedures using a known-, well tested-material. Then the efforts were to focus on the growth of *InGaAs*.

The main objective of this experimental work was the growth of bulk (thick), high quality single crystals with uniform crystal composition. For this purpose, over sixty growth experiments were performed during this study. The magnetic field distribution in the magnet opening in the absence of the growth crucible is presented in Fig. 3.3.4. The location of the liquid zone is also shown in the figure. As can be seen, the field distribution in this region is almost uniform.

In the initial LPEE experiments, a 20-kG magnetic field level was used based on the predictions of Qin and Dost [1996]. It was realized that this level of magnetic field was very strong, and the growth results were not successful. The applied magnetic field intensity was gradually lowered, and successful growth was first achieved at 4.5 kG. A number of experiments were performed at this level. We have also performed experiments at 1.0 and 2.0 kG levels to study the effect of the applied magnetic field on the growth rate.

Details of the experimental results can be found in Sheibani et al. [2003a]. All the grown crystals were single crystals. As mentioned earlier, in the LPEE set up used, the grown crystal and the liquid solution could not be separated at the end of an experiment. Therefore, a secondary growth (like an LPE growth) occurs during the cooling period in the experiments that were stopped earlier (before depleting all the solution put in the growth well). Some experiments

were stopped before depleting the solution for the purpose of determining the growth rate accurately.

Most of the crystals were grown under low current density levels (3, 5, and 7 A/cm<sup>2</sup>). Two sample crystals are shown in Fig. 3.3.5. Attempts at higher electric current density levels have not produced good crystals. It must be mentioned that it is possible to use higher electric current densities (higher than 7 A/cm<sup>2</sup>) in the growth of thin layers, as reported in the literature (for instance, Imamura et al. [1979]).

Experiments were conducted for various growth periods (from 1 to 8 days) at a temperature of 800°C. The results are summarized in Fig. 3.3.6a. As can be seen, the average thickness of the grown crystals is proportional to the applied electric current density. As expected, the thickness increases with time. It was concluded previously (Bryskiewicz et al. [1987], and Bryskiewicz and Laferriere [1993]) that the growth rate in LPEE is a linear function of the applied electric current density. The results shown in Fig. 3.3.6b indicate that this is approximately the case at the low electric current density levels, but that there is a slight deviation from linearity (with a higher rate) at the higher electric current density levels. This deviation can be attributed to the enhanced natural convection in the solution. The increase of electric current density up to 7 A/cm<sup>2</sup> in the growth of bulk crystals by LPEE has been a significant contribution. This was possible due to the novel design features of the LPEE set up of Sheibani et al. [2003a].

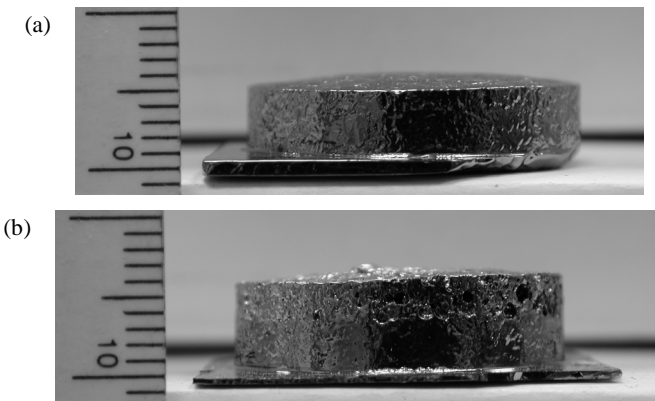


Fig. 3.3.5. Two sample crystals grown without magnetic field. In (a), all the material put into the solution well was depleted. In (b), the growth has been stopped before the depletion of the solution in order to measure the growth rate accurately, and the upper part is the secondary growth during cooling (Sheibani et al. [2003a]).

Crystals were grown at 3 A/cm<sup>2</sup>, without magnetic field, for various periods of time to determine the growth rate. Crystals were grown with thicknesses between 1.5 mm and 4.5 mm, with an average growth rate of 0.57 mm/day, as

shown in Fig. 3.3.6b. In one of the experiments a thickness of 4.5 mm was achieved in 8 days. A number of crystals were also successfully grown under the electric current densities of  $5 \text{ A/cm}^2$  and  $7 \text{ A/cm}^2$ . The growth rates were 0.75 mm/day (2.25 mm thickness in 3 days) and 1.25 mm/day (3.75 mm thickness in 3 days), respectively. It must be mentioned that some of the growth thicknesses were not representative for calculating the growth rate since in such experiments the source material put in the well was completely depleted before stopping the growth (Fig. 3.3.5a). Those experiments were not included in the calculation of growth rates.

As mentioned earlier, in order to suppress the natural convection in the liquid solution for the purpose of prolonging and stabilizing the LPEE growth process for growing bulk single crystals (thicker crystals), an applied static magnetic field was used. Two samples of grown crystals are shown in Fig. 3.3.7.

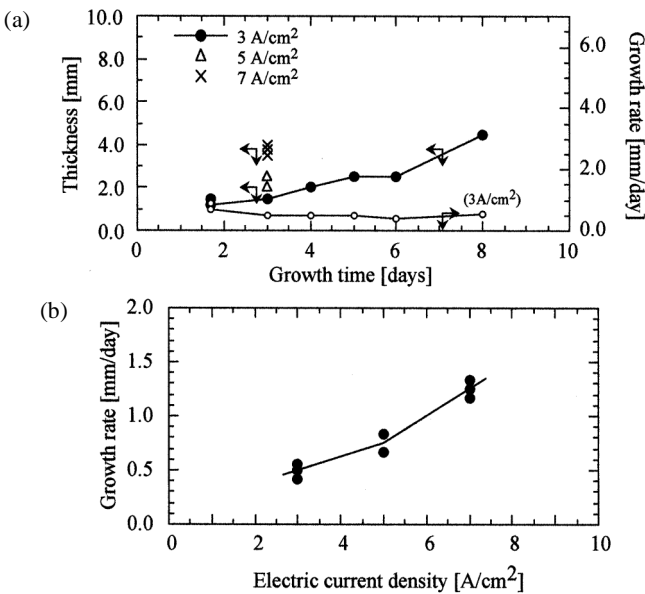


Fig. 3.3.6. Summary of the LPEE growth rates (Sheibani et al. [2003a]).

The static applied magnetic field induces a magnetic body force acting on the moving particles of the liquid solution. The combined effect of the magnetic and gravitational body forces suppresses convection and prolongs growth. This beneficial effect of an applied magnetic field was the initial intention of the present research program. This goal was successfully achieved, by growing thick single crystals. However, the unexpected effect (a very positive effect of course) of the applied magnetic (at 4.5 kG and lower field levels) was the significant increase in the growth rate (about 10 times at the 4.5 kG level, see Fig. 3.3.8a and 3.3.8b). The growth average rates were calculated at specific

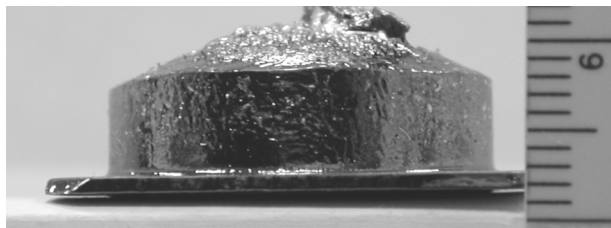


Fig. 3.3.7. A sample crystal grown at the  $J = 3 \text{ A/cm}^2$  electric current density and  $B = 4.5 \text{ kG}$  magnetic field level (after Sheibani et al. [2003a]).

electric current density levels based on the selected representative experiments that were stopped deliberately before depleting the source material. This increase in the growth was almost the same at each of three electric current density levels, namely about 6.1, 7.8, and 10.5 mm/day at  $J = 3, 5, 7 \text{ A/cm}^2$ . Such a drastic increase in the growth rate elevates the LPEE growth process to the category of a bulk growth. Growth rates at the  $B = 1.0$  and  $2.0 \text{ kG}$  levels were also higher, about 1.62 and 2.35 mm/day, respectively. Results show that the growth rate is also proportional with the applied magnetic field level (Fig. 3.3.9).

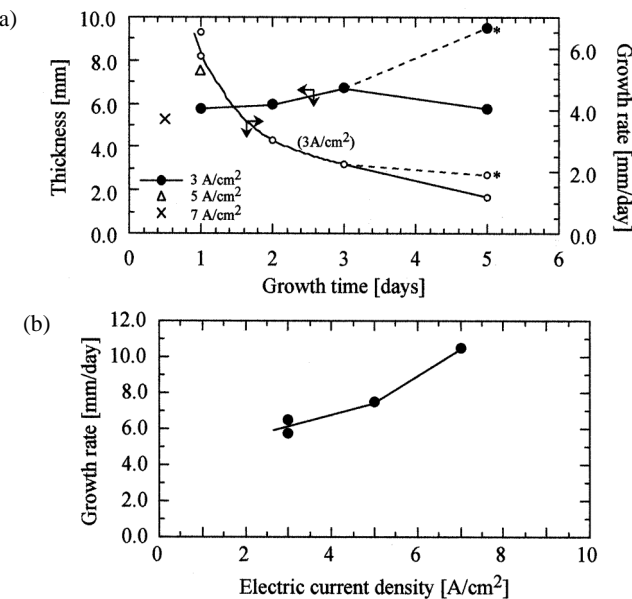


Fig. 3.3.8. Summary of the growth rates at the  $B = 4.5 \text{ kG}$  magnetic field level (after Sheibani et al. [2003a]).

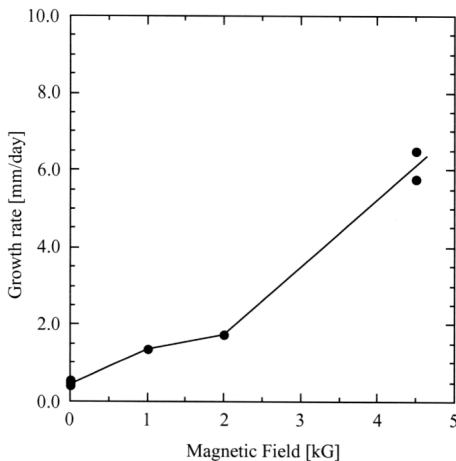


Fig. 3.3.9. Growth versus magnetic field intensity at  $J = 3 \text{ A/cm}^2$  (Sheibani et al. [2003a]).

In some experiments, the source was allowed to completely deplete to obtain the maximum thickness. These experiments are not representative of the growth rate since the materials put in the source were completely depleted. However, they were conducted to see how thick crystals could be grown. A crystal of thickness of about 9.0 mm was grown in one day using the current density of 5  $\text{A/cm}^2$ . In this run, the material in the source was completely depleted. With the design of a new, larger crucible, the growth of larger crystals may be possible. To justify that such a new design would be capable of growing crystals thicker than 9.0 mm, the current density was increased to 7  $\text{A/cm}^2$  in another experiment. All the source material was depleted, and a crystal of about 9.0 mm thickness was achieved in just 1/2 day, which is a remarkable achievement for LPEE growth.

The crystal shown in Fig. 3.3.7b has a dome-shaped surface. This is because the crystal in later stages of the growth simply took the inner shape of the crucible since we had used more source material than the liquid zone could accommodate. All of these crystals were completely single crystals all the way to the top surface.

### *Indium Composition*

The *In* composition distributions along the growth and radial directions in the grown  $\text{Ga}_{1-x}\text{In}_x\text{As}$  ( $x=0.04$ ) crystals were measured by Electron Micro Probe Analysis (EPMA) and Energy Dispersive X-ray Spectroscopy (EDX). Wafers were prepared from the grown crystals and the surfaces were etched in bromine-methanol solution (5-10% bromine). Samples from a total of 13 crystals were

analyzed. Results were almost the same for all of these crystals, and therefore only a few are presented here.

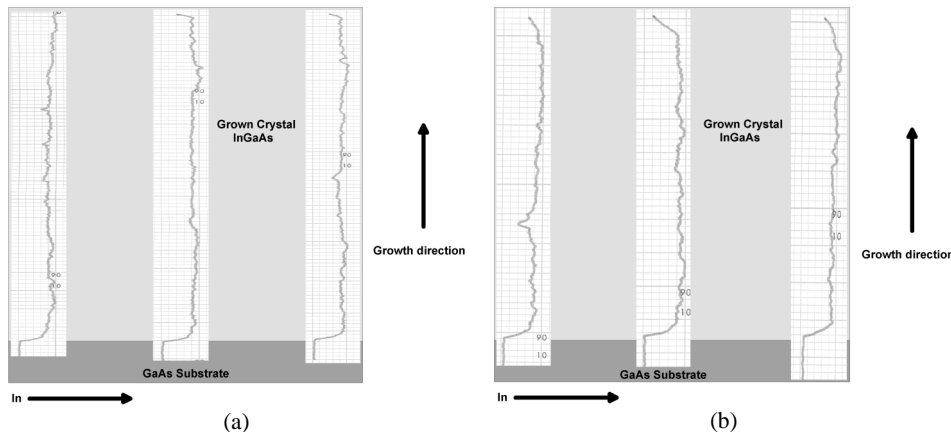


Fig. 3.3.10. The *In* composition distribution in the grown crystals. EPMA and EDX analyses were carried out by Professor Akira Tanaka of Shizuoka University, Hamamatsu, Japan. (a) at  $J = 5 \text{ A}/\text{cm}^2$ ,  $B = 0.0 \text{ kG}$ , and *Growth Period* = 3 days, and (b)  $J = 5\text{A}/\text{cm}^2$ ,  $B = 4.5 \text{ kG}$ , and *Growth Period* = 1 day (after Sheibani et al. [2003a]).

Fig. 3.3.10 shows the *In*-composition distribution along the growth direction in the grown GaInAs crystals by using the EPMA. The growth conditions were  $J = 5\text{A}/\text{cm}^2$ ,  $B = 0.0 \text{ kG}$ , and *Growth Period* = 3 days for the results presented in Fig. 3.3.10a, and  $J = 5\text{A}/\text{cm}^2$ ,  $B = 4.5 \text{ kG}$ , and *Growth Period* = 1 day for the results presented in Fig. 3.3.10b. Both characterization results indicate that a uniform distribution of about 4%-*In* can be achieved in the regions of about 1.5–2.5 mm-thickness from the substrate. A slight decrease of the Indium around the top surface of the crystal can be seen because of the lack of source materials.

Fig. 3.3.11 shows the results of the EDX measurement. The grown conditions were  $J = 3 \text{ A}/\text{cm}^2$ ,  $B = 0 \text{ kG}$ , and *Growth Period* = 4 days for Fig. 3.3.11a and  $J = 3 \text{ A}/\text{cm}^2$ ,  $B = 0 \text{ kG}$ , and *Growth Period* = 5 day for Fig. 10b. Uniform distributions of the *In* composition were also obtained along both the growth and radial directions.

The results of Sheibani et al. [2003a] suggest that the LPEE growth technique has a great potential in growing ternary bulk and single crystals with superior compositional uniformity as desired in the device industry. Advances made through this work may be considered as significant initial steps towards the commercialization of the LPEE technique for growing high quality, bulk single crystals with uniform compositions.

The ELO growth of semiconductors by LPEE is presented in Chapter 6 together with its modeling for the sake of efficiency.

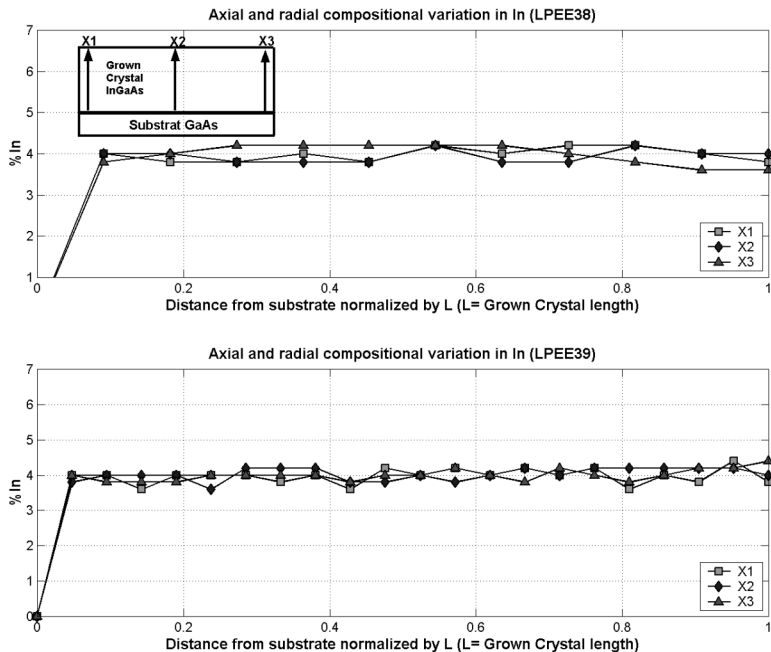


Fig. 3.3.11. Distribution of the *In* composition in the grown crystal by EDX. The growth conditions were  $J = 3 \text{ A/cm}^2$ ,  $B = 0 \text{ kG}$ , and *Growth Period* = 4 days for the top figure, and  $J = 3 \text{ A/cm}^2$ ,  $B = 0 \text{ kG}$ , and *Growth Period* = 5 day for the bottom.

### 3.4. Traveling Heater Method

The traveling heater method (THM) is a solution growth technique, which allows the preparation of bulk monocrystalline mixed-compound semiconductors. THM can be used to produce non-congruent melting materials, including families of ternary and quaternary II-VI and III-V compounds, which can not be grown adequately by standard melt growth techniques. Since the process is conducted below the melting point of the semiconductor, relatively low temperatures are involved, which reduces contamination and vapor pressure related problems. This leads to bulk crystals with improved dopant homogeneity, reduced dislocation densities, and excellent electrical properties (Benz and Mueller [1979], Benz [1985], Bishopink and Benz [1993]). Compound semiconductor materials such as GaAs and GaSb exhibit a finite phase field over a significant temperature range below the melting point, leading to an excess of one constituent element occupying sites of the other element in the crystal lattice (so-called *anti-sites*), or, in extreme cases, the formation of precipitates of the excess element, due to the high degree of

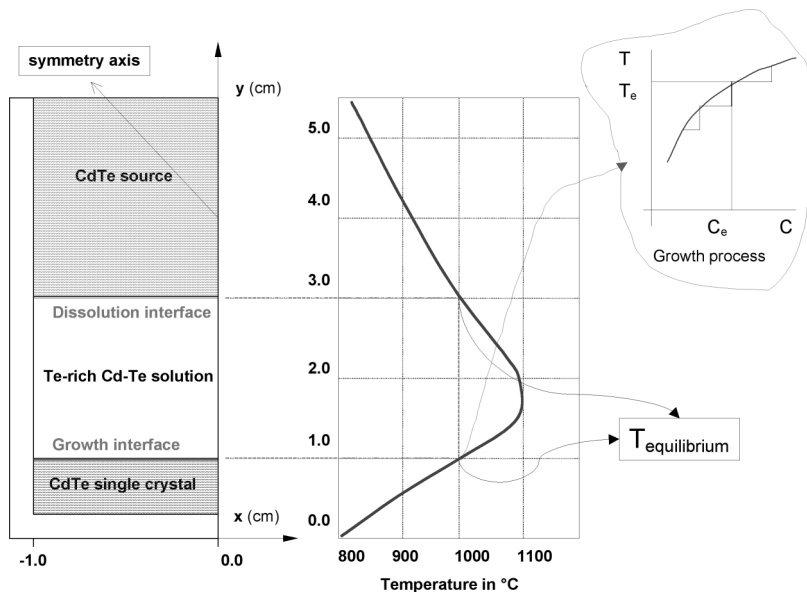


Fig. 3.4.1. Schematic view of a THM growth system (*CdTe*), and the applied temperature profile in thermal equilibrium.

retrograde solid solubility. As a result, it is impossible to obtain precisely stoichiometric compounds by conventional melt growth techniques. By growing from solution at temperatures below the lower limit of the composition phase field it is therefore conceivable that one could produce, for example, highly stoichiometric intrinsic *GaSb* as an alternative substrate to Cadmium Zinc Telluride (*CdZnTe*) for the epitaxial growth of Mercury Cadmium Telluride (*HgCdTe*) Focal Plane Array thermal imaging applications. The traveling heater method is also gaining acceptance as a viable production process for the growth of large diameter (in excess of 75mm) single crystal *CdZnTe* as a room temperature solid state detector for nuclear medical imaging applications.

Materials which would normally dissociate before melting may also be synthesized by THM from a suitable solvent. In general, such materials are typically oxide-based, non-semiconducting, and unsuited as candidates for growth from metallic solutions.

### 3.4.1. Experimental THM Growth Process

THM uses a moving axial temperature gradient as the driving force to transfer polycrystalline feed at a controlled rate to re-crystallize on a seed, thus growing monocrystalline material of the same average composition as the feed. A schematic diagram of the THM process is shown in Fig. 3.4.1, together with the axial thermal profile of the furnace. A schematic view of the THM growth

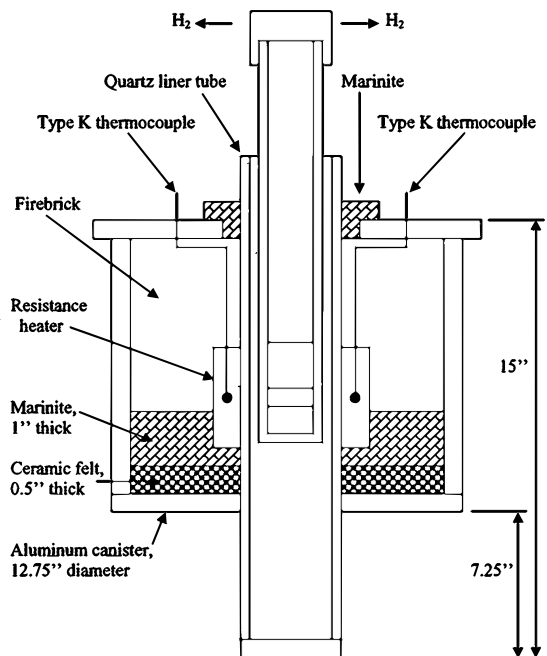


Fig. 3.4.2. Schematic view of the THM-growth system of Amistar Research Inc. (after Meric et al. [1999]).

system of Amistar Research Inc. of Victoria, BC, Canada, is also shown in Fig. 3.4.2.

The apparatus consists of a quartz ampoule at the bottom of which is placed a single crystal seed of the desired composition and crystallographic orientation. This is surmounted by an appropriate amount of solvent material, preferably one of the constituent elements of the material to be grown; generally, *Ga* for the growth of *GaSb* or *GaInAs*, *Te* for the case of *CdZnTe*. This is followed by a fine grained polycrystalline source material with the same average composition as that of the seed. After sealing under vacuum or an inert gas (if necessary), the ampoule is then placed in a furnace consisting of a concentric heat source positioned to surround the solvent zone. The operating temperature and the amount of solvent material are determined by the relevant phase diagram such that the solvent will be saturated at typically 20 mole percent of the desired composition and the particular axial gradient. Precise location of the ampoule and charge, relative to the heater, ensures that a portion of the seed and of the source material will dissolve until the solvent reaches saturation and a dynamic equilibrium is established. The ampoule is then slowly lowered through the hot

zone at a controlled rate, with or without rotation of the ampoule. As a consequence of the narrow heater profile, the temperature at the seed-solvent interface reduces and the melt becomes locally supersaturated and crystallization occurs. Simultaneously, the temperature at the dissolution interface increases and more of the source material dissolves.

Growth rates for THM are typically over an order of magnitude less than those associated with melt growth techniques. The growth rate in THM is limited by the transport rate of the slowest constituent species through the solution zone and by the morphological instability of the growth interface caused by constitutional supercooling (Mueller and Neumann [1983]). Interfacial breakdown resulting in solvent inclusions and polycrystallinity occurs if the growth rate, which is given in steady state by the relative velocity of the heater with respect to the charge, is chosen too high.

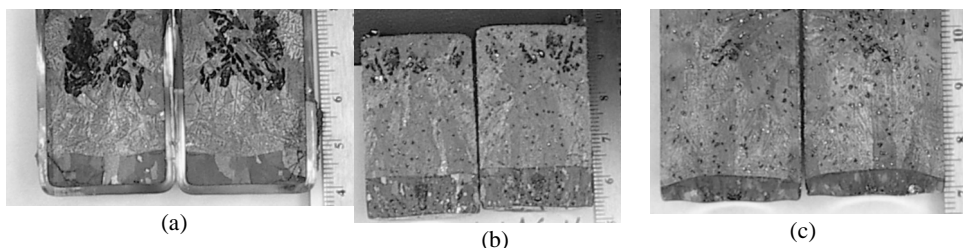


Fig. 3.4.3. Thermal signature of a THM furnace under various heat extraction conditions, obtained from quenching experiments (Liu et al. [2003]).

In THM, the speed of the heating profile and the growth rate must be controlled so as to lead to the growth of high quality crystals. Uniform growth in the growth direction (i.e., a flat interface) is desirable because it leads to single crystals of uniform composition and also less defects. As it is very difficult, if not impossible, to experimentally achieve such a perfection, a slightly convex growth interface is preferable for single-crystalline growth in order to eliminate peripheral grains. This can be achieved by an optimum thermal design for the THM growth crucible. The shape of the interface can be controlled by controlling the heat transfer in the system. For instance, thermal signatures taken in the THM system of Liu et al. [2003] show that the shape of the growth interface can be controlled to provide a favorable growth interface shape (see Fig. 3.4.3.).

The initial thermal signature experiments were carried out with the quartz ampoule resting directly on the aluminum shaft on the lowering platform (see Fig. 3.4.3). The furnace temperature was then ramped to 900 °C, the temperature used in the THM-I prototype furnace, in which the ampoule is suspended from above by a lowering mechanism. Examination of the ampoule showed that very little of the feed material had dissolved in the solvent, and that excessive

cooling of the ampoule had occurred, as a result of heat extraction by the aluminum support shaft. A thermal break, in the form of a 25-mm long 25-mm diameter cylinder of refractory insulation material, was then positioned between the ampoule base and the supporting shaft, and the thermal signature obtained. A vertical section of the resulting charge is illustrated in Fig. 3.4.b. It can be seen that approximately 5mm of polycrystalline CZT had formed at the base of the ampoule, with a slightly concave growth interface shape. Further modifications were made to the thermal insulation to control the radial distribution of the axial heat flow in order to obtain the more desirable planar or slightly convex profile required to promote single crystal growth.

### 3.4.2. THM Growth Under Rotating Magnetic Fields

Preliminary experiments have been performed at the University of Victoria in a custom designed THM furnace equipped with a rotating magnetic field (RMF) generator to study the effects of a small (50G) rotating magnetic field on improving mixing within the solvent zone, and to allow a significant increase in the maximum growth rate (i.e. the translation rate of the ampoule) before the onset of interface breakdown and polycrystalline growth (Redden et al. [2005]). Even under conditions of multi-grained seeds the application of a rotating magnetic field allows an increase of growth rate up to 4 times that in the absence of RMF mixing, with a continuously increasing dominant central grain until complete exhaustion of the polycrystalline source material.

A view of THM-I furnace of CGL at the University of Victoria is shown in Fig. 3.4.4.

Rotating magnetic fields have also been used by Salk et al. [1994], and Senchenkov et al. [1999], to improve the quality and compositional uniformity, and to increase growth rate by a factor of 2-4 times, for the THM growth of *CdTe* and *CdTe<sub>0.9</sub>Se<sub>0.1</sub>*, and *HgCdTe*, respectively.

Recent work by Gelfgat et al. [1999] has demonstrated by both simulation modeling and experimentation, that a combination of different, independent magnetic fields may be used simultaneously to provide wide possibilities for controlling the parameters of convection and heat/mass transfer in crystal growth processes. Stationary and non-stationary fields may be combined to target a specific growth situation.

### 3.4.3. The Cold Traveling Heater Method

One of the problems associated with the THM growth of materials such as *CdTe* and *CdZnTe* lies in the difficulty in producing adequate quantities of polycrystalline feed material. These materials have very high vapor pressures at their melting points, and must be grown in high pressure Bridgman furnaces. In the case of ternary compounds such as *CdZnTe* this is further complicated by the fact that the composition of the resultant ingot will vary continuously as a result of the large separation between the solidus and liquidus pseudo-binary

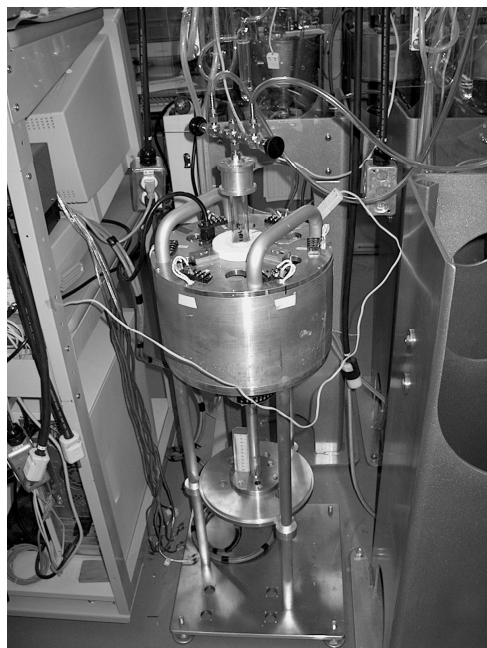


Fig.3.4.4. A view of THM-I Furnace of CGL at the University of Victoria.

phase diagram. This may be overcome for small charge sizes by rapid quenching from the molten state, but is limited by the rate at which heat may be extracted from the central region of the ingot. For large diameters, typically in excess of 25mm diameter, coring will occur, leading to highly porous feed material of inconsistent and unpredictable composition. The use of such material as source for THM growth will lead to corresponding compositional inhomogeneity.

To overcome this problem Triboulet et al. [1990] , El Mokri et al. [1994] have developed the so-called Cold Traveling Heater Method (CTHM), whereby the source material (*CdTe*) is synthesized *in situ*. This is achieved by inserting a cylindrical rod of cadmium surrounded by a stoichiometric amount of crushed tellurium particles above the Te solvent layer. *CdTe* is thus synthesized and dissolved in the solvent as the liquid zone becomes depleted as growth progresses. A review of the fundamentals of the synthesis of *CdTe*, including the CTHM concept, has also been given by Triboulet [2004] for the growth of ternary alloys.

The CTHM concept has been further developed by Reig et al. [2001] for the growth of Mercury Manganese Telluride (*HgMnTe*), a diluted magnetic semiconductor with potential applications as detector and laser elements controlled by a magnetic field. Ingots of *HgTe* and *MnTe* are first prepared by

CTHM and THM, respectively. Ingots of each material are then sectioned vertically with cross sectional areas corresponding to the desired  $HgMnTe$  composition and placed face to face and processes by CTHM. A compositional homogeneity of better than 1% along the whole length of the  $HgMnTe$  crystal was demonstrated by accurate lattice parameter, band edge (FTIR) and magnetic susceptibility measurements.

### 3.5. Liquid Phase Diffusion

In this section we present a new crystal growth technique, called *Liquid Phase Diffusion* (LPD) which was first developed by Nakajima et al. [1999] under the name of *Multicomponent Zone Melting* (MCZM), and later utilized by Yildiz et al. [2005]. We introduce the essential features of this technique and some experimental results. This method is mainly used for the growth of  $Si_xGe_{1-x}$  crystals, therefore the emphasis will be on  $Si_xGe_{1-x}$ . The recent developments in modeling of this growth process are discussed in Chapter 8.

#### 3.5.1. Introduction

Research on  $Si_xGe_{1-x}$  alloys dates back to as early as 1954 (Jonhson and Christian [1954]). However, a significant body of research associated with the growth of high quality  $Si_xGe_{1-x}$  single crystals started coming into existence approximately two decades ago. Since its composition can be tailored to obtain the desired material properties, and it can easily be integrated with the well-developed and long-existing silicon technology,  $Si_xGe_{1-x}$  is a promising candidate for a variety of device applications such as a base in  $Si/SiGe$  heterojunction bipolar transistors (HBT) (Cressler [1995], Paul [1999]), high electron mobility field effect transistors (Mii et al. [1991], photodetectors (Jutzi and Berroth [2000]), solar cells (Healy and Green [1992], Fitzgerald et al. [1992], Said et al. [1999], Nakajima et al. [1999]), thermoelectric power generators (Bhandari and Rowe [1980], Slack and Hussein [1991]), tunable neutron and  $x$ -ray monochromators (Kozhukh et al. [1983]), high speed temperature sensors, and  $\gamma$ -ray detectors (Schilz and Romanenko [1995]).

$Si_xGe_{1-x}$  single crystals for device applications have generally been prepared in the form of thin films grown on a silicon substrate by various epitaxial growth techniques such as Molecular Beam Epitaxy (MBE) (Luo et al. [2001]), Rapid Thermal Chemical Vapor Deposition (RTCVD) (Fitzgerald et al. [1991]), Chemical Vapor Deposition (CVD) (Bhattacharya et al. [1991]), and Ultra High Vacuum Chemical Vapor Deposition (UHV/CVD) (Meyerson et al. [1994]). However, when a  $Si_xGe_{1-x}$  alloy is epitaxially deposited on a silicon substrate, the alloy layer is compressively strained. When the thickness of the strained layer exceeds a critical value, misfit and threading dislocations develop to relieve the built-in compressive strain. The existence of misfit and threading dislocations reduces the mobility and electronic quality of the crystal (Paul

[1999]). The critical layer thickness decreases significantly with the increasing germanium content. However, most of the applications require a much thicker  $Si_xGe_{1-x}$  layer with a high germanium content.

Due to the above mentioned difficulties, the growth of high quality and compositionally uniform  $Si_xGe_{1-x}$  substrates is desirable. To this end, a variety of melt crystal growth techniques, such as Czochralski (Cz) (Abrasimov et al. [1997], Matsui et al. [1998], Kurten and Schils [1994], Yonenaga and Nonaka [1998]), floating zone (FZ) (Wollweber et al. [1996]), Bridgman (Dold et al. [1998], Dahlen et al. [1994]), multi component zone melting (Nakajima et al. [1999]), and liquid encapsulated zone melting (Bliss et al. [1997]), have been utilized. However, these melt techniques exhibit challenges in the growth of single crystals of uniform composition and low defect densities. This is mainly due to the large miscibility gap in the phase diagram of  $Si_xGe_{1-x}$ . Thus, a small change in the solidification rate may lead to significant composition variations, and growth striations in the grown crystals (Abrasimov et al. [1997], Matsui et al. [1998], Wollweber et al. [1996], Dold et al. [1998], Dahlen et al. [1994]). In addition, the significant differences in the physical properties of *Si* and *Ge*, such as density, melting temperature, and lattice parameter, add additional difficulties.

In order to produce crystals with uniform compositions, Nakajima et al. [1999] developed the multicomponent zone melting (MCZM) technique for the growth of  $Si_xGe_{1-x}$  crystals. This technique was also extended to grow *InGaAs* crystals by Nishijima et al. [2000]. Furthermore, Azuma et al. [2001] and Sasaki et al. [2002] developed an in-situ experimental observation system for the growth of  $Si_xGe_{1-x}$  by the MCZM technique to control interface position and temperature.  $Si_xGe_{1-x}$  crystals from the silicon side (on silicon seed) have also been grown with uniform compositions using the MCZM technique by Nakajima et al. [2002]. An automatic feedback control system for the MCZM method was developed by Azuma et al. [2003] to track the crystal–melt interface position in order to keep the temperature at the interface constant during growth. It was used successfully to grow *Ge*-rich  $Si_xGe_{1-x}$  bulk crystals with uniform compositions. Nishijima et al. [2004] and Usami et al. [2005] also introduced zone techniques for the growth of crystals with uniform compositions.

In the above mentioned methods, the crystal composition will not be uniform in the growth direction, if the system is kept stationary. In order to grow crystals with uniform compositions, the liquid zone (melt or solution) has to be moved at a very precise rate. Even so, the crystal composition may fluctuate since it is very difficult to have exact match between the natural mass transport rate of the system and the translation rate.

Solution growth techniques, such as LPEE and THM offer, in principle, a better controllability of the crystal composition. Particularly in LPEE the growth rate is the natural mass transport rate imposed by the applied electric current (electromigration). However, LPEE requires a seed of single crystal of

the same composition of the crystal to be grown. It is difficult to acquire the needed seed crystals with desired compositions, particularly crystals with higher compositions.

In order to address this issue, the LPD technique has been utilized by Yildiz et al. [2005] for the growth of  $Si_xGe_{1-x}$  crystals. There were two main objectives in mind. The first was the growth of bulk  $Si_xGe_{1-x}$  single crystals with varying composition from which the seed substrates with required compositions can be extracted. The second objective was the development of the first stage of a hybrid growth technique that may combine LPD and LPEE in a single process. In this hybrid technique in mind, a graded single crystal would be grown by LPD up to the composition of interest, and then at this stage the LPEE process would be initiated by passing an electric current through the growth system at a uniform furnace temperature, leading to the growth of single crystals with desired uniform compositions. Such a single process would eliminate the adverse affects of growing crystals in two stages.

### *3.5.2. Multicomponent Zone Melting Method*

As mentioned earlier, Nakajima et al. [1999] developed an improved growth technology (MCZM) to grow *Ge-rich*  $Si_xGe_{1-x}$  crystals on *Ge*, based on the multi-component zone melting method developed by Nakajima and Kusunoki, [1996], and Suzuki et al. [1996]. The graded  $Si_xGe_{1-x}$  crystals with a gradually increasing *Si* composition were grown through continuous oversupply of the *Si* solute to the growth melt (Nakajima and Kusunoki, [1996], Nakajima et al. [1991]). The supply of *Si* supercools the melt near the growth interface and raises the growth temperature. In order to grow  $Si_xGe_{1-x}$  crystals with uniform compositions, the temperature at the growth interface must be constant. This was achieved by controlling the rising liquidus temperature (due to supply of *Si* into the melt) by pulling down the growth crucible to the cooler region. It was shown that the uniform (top) section of the prepared  $Si_xGe_{1-x}$  single crystal is suitable as a lattice-matched seed for the subsequent growth of *GaAs*.

#### *Growth of $Si_xGe_{1-x}$ from the Ge-side*

Fig. 3.5.1 illustrates the MCZM apparatus. In order to grow the  $Si_xGe_{1-x}$  crystal on a *Ge* seed, a constant supply of *Si* from the source is required. This is achieved by a temperature profile that has a uniform zone at the top and a rapidly cooled zone with a large temperature gradient at the lower region.

A 1.0 cm-thick (100)*Si* single crystal as the source material at the top, two 1 cm-thick (100)*Ge* single crystals for the growth melt in the middle, and a 1 cm-thick (100)*Ge* single crystal as seed at the bottom are placed in a quartz crucible of 1.5 cm in diameter. Then, the structure is sealed in the quartz ampoule in high vacuum as shown in Fig. 3.5.1a. The crystal diameter is 1.5 cm. A carbon block is placed at the top of the *Si* source as a stopper (weight). The *Si* and *Ge* crystals used were undoped, and of purity of ~10 nines. At the initial growth

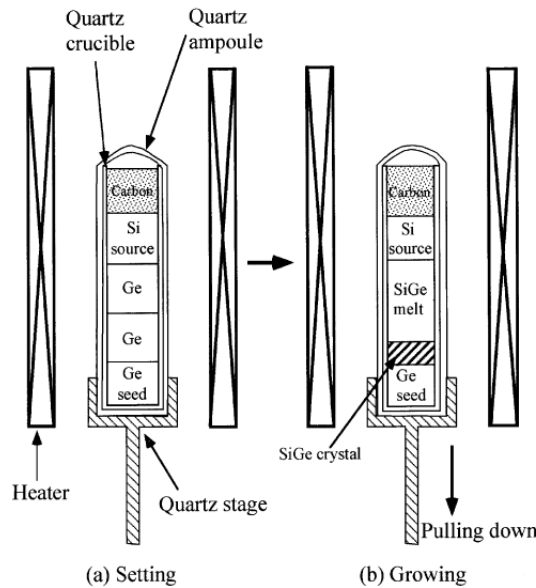


Fig. 3.5.1. The MCZM apparatus with a quartz crucible in a quartz ampoule showing (a) initial placement of *Si* and *Ge* crystals and (b) growing *SiGe* crystal (after Nakajima et al. [1999]).

temperature, a part of the *Si* source, the two *Ge* crystals, and a part of the *Ge* seed melt, and form the *Si-Ge* growth melt (a binary liquid solution mixture) as shown in Fig. 3.5.1b. Under the effect of the applied temperature profile, *Si* continuously dissolves into the solution and diffuses towards the *Ge* seed according to the phase diagram of the *Si-Ge* system, and forms a concentration gradient of *Si* in the solution as shown in Fig. 3.5.2.

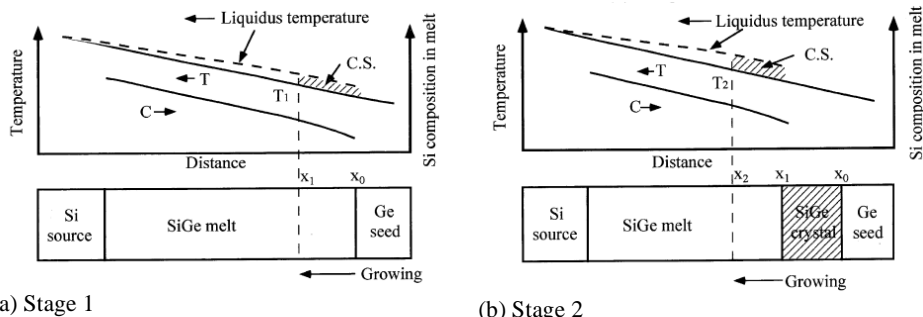


Fig. 3.5.2. Schematic representation of the temperature profile in the furnace, *Si* concentration profile in the *Si-Ge* solution (melt), and liquidus temperature of the solution during (a) Stage 1 and (b) Stage 2. C.S. stands for constitutional supercooling (after Nakajima et al. [1999]).

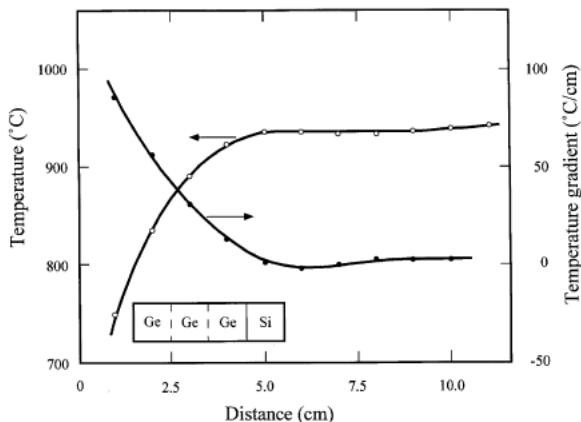


Fig. 3.5.3. Typical furnace temperature profile and temperature gradient (after Nakajima et al. [1999]).

Fig. 3.5.2 illustrates the temperature profile, the *Si* concentration profile, and the liquidus temperature corresponding to the *Si* concentration in the *Si-Ge* solution. Under stationary growth conditions (i.e., without pulling down the crucible), the initial stage (Stage 1), and a later stage (Stage 2) are shown schematically in Figs. 3.5.2a and 3.5.2b, respectively. The growth process is as follows.

According to the *Si-Ge* phase diagram, the *Si*-source dissolves into the *Si-Ge* solution, and then the *Si* species move towards the growth interface. This increases the *Si* concentration in the solution near the growth interface, and consequently the liquidus temperature in this region becomes higher than the actual liquid (melt) temperature, giving rise to a constitutional supercooling in the solution. During Stage 1, the *SiGe* crystal grows (on *Ge*) by constitutional supercooling. The amount of the constitutional supercooling decreases as the growth interface progresses, and the liquid temperature near the surface increases. In Stage 2, as the growth interface moves up, towards the higher *Si* concentration region (closer to the *Si* source), the degree of constitutional supercooling increases. This leads to a continuous growth. The required constitutional supercooling for growth is maintained by the continuous supply of *Si* species from the source. This process can be better understood by examining the *Si-Ge* binary phase diagram. The liquidus temperature of the solution near the interface becomes higher along the liquidus curve as the crystal grows. The *Si* composition (*x*) in the growing  $\text{Si}_x\text{Ge}_{1-x}$  crystal increases as the growth temperature becomes continuously higher, leading to a crystal with a graded *Si* composition.

However, in order to obtain a uniform composition, the temperature at the interface must remain constant. This is achieved by moving the crucible to the

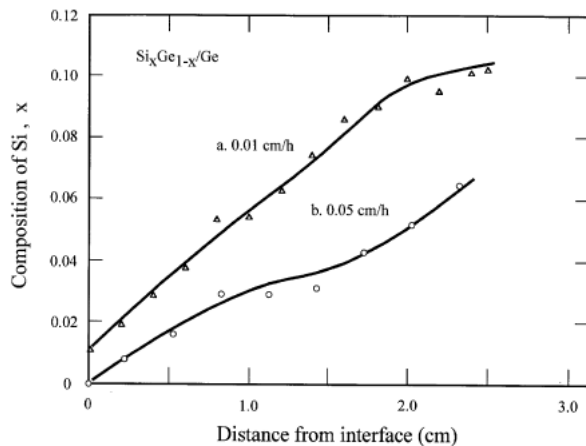


Fig. 3.5.4.  $\text{Si}$  composition variation in the  $\text{Si}_x\text{Ge}_{1-x}$  graded crystals grown at the pulling rates of 0.01 (a) and 0.05 (b) cm/h, and growth times of 59 hours (a) and 50 hours (b) (after Nakajima et al. [1999]).

colder region (by pulling down the crucible), by maintaining the growth rate (mass transport at the growth interface) matched as closely as possible to the pulling rate. Then, the  $\text{Si}$  composition variation in the crystal can be minimized. The temperature profile and temperature gradient of the furnace used are presented in Fig. 3.5.3.

The temperature profile with a constant temperature gradient was developed

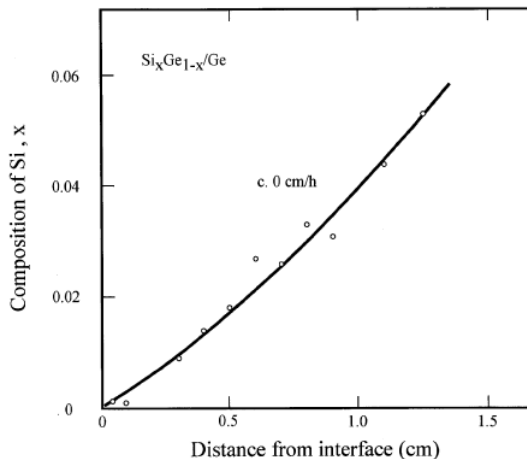


Fig. 3.5.5.  $\text{Si}$  composition variation in the  $\text{Si}_x\text{Ge}_{1-x}$  graded crystal grown without pulling with a growth time of 15 hours (after Nakajima et al. [1999]).

as follows. The initial position of the *Si* and *Ge* crystals prior to pulling is shown in Fig. 3.5.3. The temperature of the uniform zone is set at about 940°C, and the maximum temperature gradient in the rapidly cooled zone is more than 80°C/cm. The *Si* concentration in the solution is strongly affected by the heater temperature of the uniform zone. The growth system inside the furnace was rapidly heated up to the heater temperature of 935°C, and thereafter the heater temperature was kept constant.

Figs. 3.5.4 and 3.5.5 show the *Si* composition in the grown  $Si_xGe_{1-x}$  crystals (a, b and c) as a function of the distance from the *SiGe/Ge* interface, determined by an energy dispersive x-ray (EDX) analysis on the  $Si_xGe_{1-x}$  crystals cut along the (100) planes in the growth direction. As seen in Fig. 3.5.4a, the composition of *Si* increases along the growth direction. The variation in composition decreases with the increasing pulling rate, as expected (see Fig. 3.5.4 and 5).

As seen in Fig. 3.5.6, at the pulling of 0.08 cm/h the *Si* composition in the grown crystal becomes almost uniform, reaching a composition value of  $x = 0.02$  at the distance of 0.5 cm from the growth interface. The growth time to reach this composition is about 6 hours. The initial portion of the crystal with graded composition was grown for 6 h (with no pulling), and then the section with a uniform composition was achieved at the pulling rate of 0.08 cm/h for 44 h. Fig. 3.5.6 shows the compositional profile of the crystal.

The photograph of a cross-section (100) cut of a  $Si_xGe_{1-x}$  crystal (in the growth direction) is shown in Fig. 3.5.7. The sections of the *Ge*-seed, the grown  $Si_xGe_{1-x}$  crystal, and the *Si*-source are identified on the picture. The dark, convex-shaped lines appearing in the photograph are saw marks (Nakajima et al. [1999]). As shown by Nakajima et al. [1999], the MCZM technique was successful in growing  $Si_xGe_{1-x}$  crystals on *Ge* seeds from the *Ge*-side, with

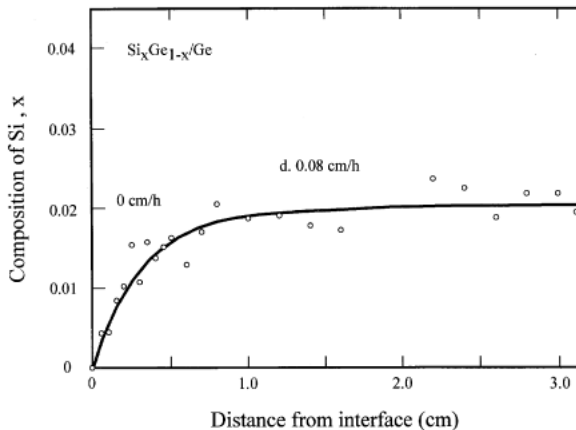


Fig. 3.5.6. *Si* composition variation in the  $Si_xGe_{1-x}$  crystal grown using pulling rates of two steps: 0 and 0.08 cm/h (Nakajima et al. [1999]).

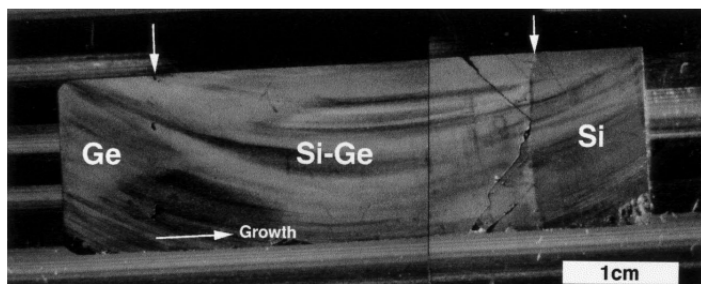


Fig. 3.5.7. Picture of a cut (100) of a  $SiGe$  crystal (in the growth direction). The arrows indicate the location of interfaces between  $Si$  and  $SiGe$  and  $Ge$  and  $SiGe$  (after Nakajima et al. [1999]).

uniform compositions. It was found that the pulling rate is the most important factor affecting the crystal composition.

#### *Growth by In-situ Monitoring*

Based on the success of the MCZM technique in growing  $Si_xGe_{1-x}$  single crystals with uniform compositions, an in-situ monitoring system was developed by Azuma et al. [2001] to observe and control the interface temperature. Such a direct monitoring was important to have a precise control of the balance between the ampoule pulling rate and the crystal growth rate, in making it possible to keep the interface temperature constant during the entire growth process. Experimental results show that the MCZM technique is capable of growing  $Si_xGe_{1-x}$  crystals with the desired compositional uniformity, which can be used as substrates for the semiconductor heterostructure technology.

In the experiments, the initial materials were stacked in the growth ampoule as being a  $Si$  single crystal source at the top, a piece of polycrystalline  $Ge$  in the middle, and a single crystal  $Ge$  substrate at the bottom. Under the applied temperature profile, the polycrystalline  $Ge$  in the middle melts completely, and the  $Ge$ -seed at the bottom melts partially. The dissolution of silicon into the  $Ge$  melt forms the  $Si-Ge$  growth solution. In the system, the growth ampoule can be pulled in the vertical direction at various rates. For a better thermal axisymmetry, the ampoule can also be rotated about the growth axis at a rate up to 10 rpm, (Fig.3.5.8). Eight thermocouples are placed spirally around the ampoule (1 cm apart) to observe the temperature profile during growth. The most important feature of this system is its ability to allow a direct observation of the growth interface, and provide information for the temperature and position of the growth interface. A 10 mm  $\times$  90 mm quartz window is designed for observation. In the system, the growth interface is visible to the naked eye. Using the visible light reflected at the beam splitter, a CCD camera (Hamamatsu C2400) records the image of the interface. The infrared radiation that goes through the beam splitter allows the temperature to be measured by a thermoviewer (Nikon LAIRD 3A). The black body carbon films inserted

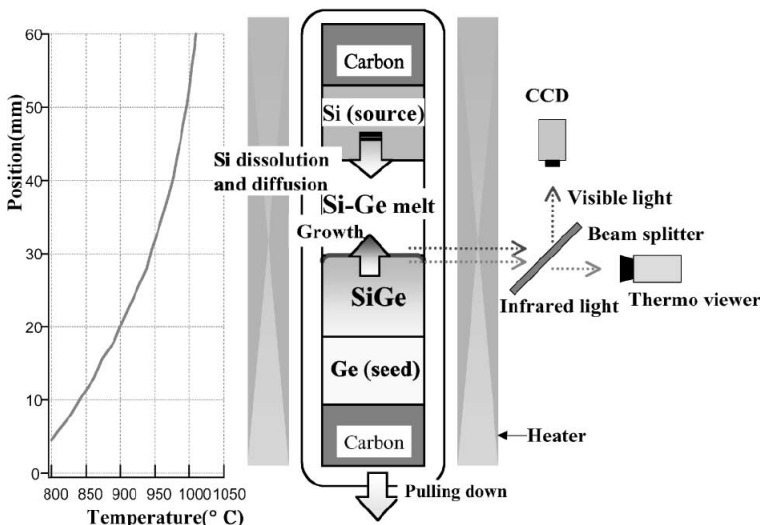


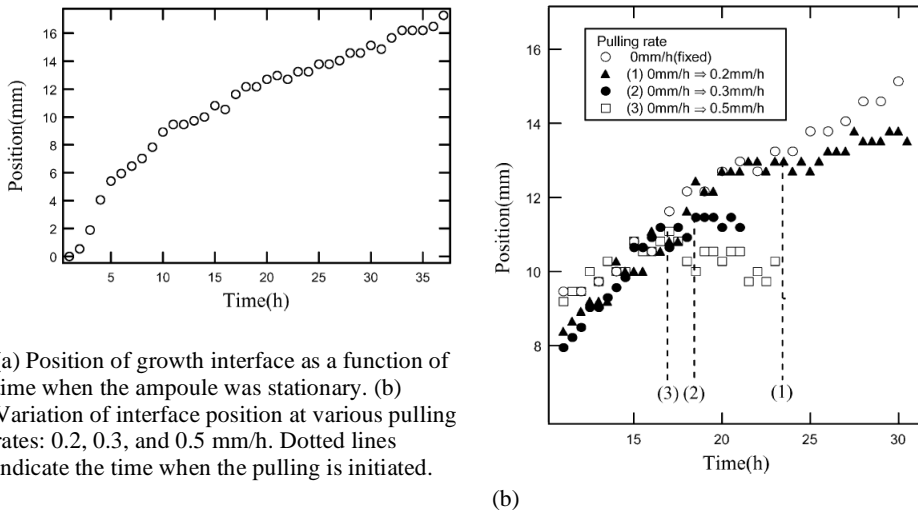
Fig. 3.5.8. The growth system of *SiGe* with an in-situ monitoring system. The applied temperature profile is shown on the left (after Azuma et al. [2001]).

between the crucible and the ampoule minimize the undesirable reflection of radiation from the heaters.

The applied temperature gradient is about  $30^{\circ}\text{C}/\text{cm}$  in the growth region (Fig. 3.5.8). The ampoule was rotated at 1 rpm during growth. Images were captured from a fixed viewpoint at a spatial resolution of about  $300 \mu\text{m}$ . A grown crystal was cut in the growth direction, and its composition was measured along the center line by EDX analysis with a probe diameter of  $20 \mu\text{m}$ .

Fig. 3.5.9a shows the position of the interface as a function of the growth time, measured when the system was stationary. As seen, the initial rapid growth is followed by an almost constant growth rate (about  $0.27 \pm 0.04 \text{ mm/h}$ , determined by the least squares method). This shows that the growth rate is far from the average growth rate (around  $0.5 \text{ mm/h}$  in the first 15-mm distance) during the most part of the growth period. The constant growth rate observed following the initial growth period is useful to determine the required pulling rate for the growth of crystals with uniform composition (Azuma et al. [2001]).

In the remaining experiments, after a 1-cm growth, samples were pulled down at the rates of 0.2, 0.3, and  $0.5 \text{ mm/h}$ . Fig. 3.5.9b presents the interface position as a function of time. At the pulling rate of  $0.3 \text{ mm/h}$ , which leads to a growth rate about  $0.27 \pm 0.04 \text{ mm/h}$ , the position seems to remain constant. However, at the pulling rates of 0.2 and  $0.5 \text{ mm/h}$ , the position exhibits small upward and downward variations, respectively. This shows that the pulling rate of  $0.3 \text{ mm/h}$  was a good match to follow the actual mass transport rate.



(a) Position of growth interface as a function of time when the ampoule was stationary. (b)  
Variation of interface position at various pulling rates: 0.2, 0.3, and 0.5 mm/h. Dotted lines indicate the time when the pulling is initiated.

Fig. 3.5.9. (after Azuma et al. [2001]).

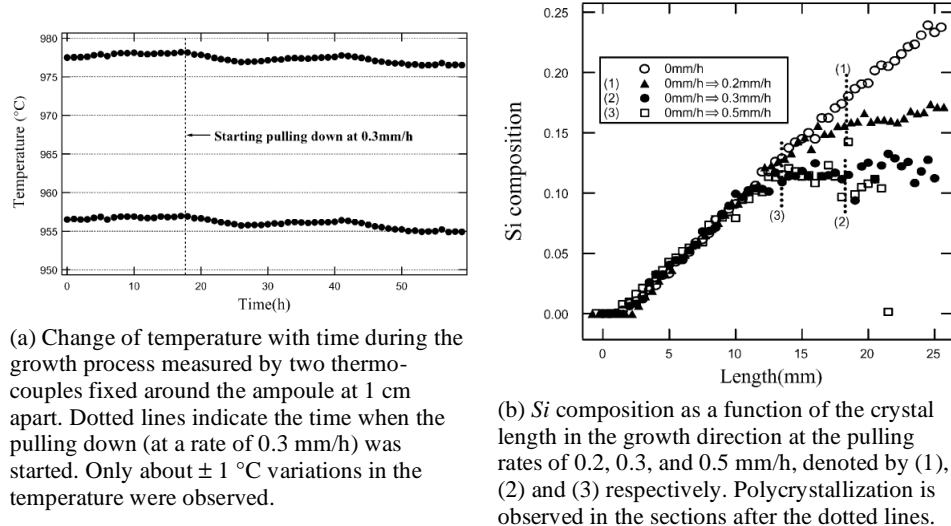


Fig. 3.5.10. (after Azuma et al. [2001]).

The variation of temperature with time is shown in Fig. 3.5.10a. Temperature was measured at two fixed positions in the furnace, by thermocouples placed around the ampoule. As can be seen, the applied temperature profile was not affected by the ampoule movement. The maximum change observed in temperature was about only  $\pm 1^\circ\text{C}$ . The interface remained almost stationary,

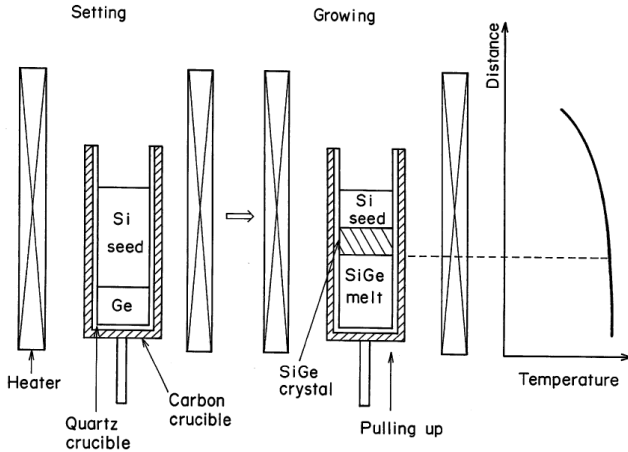


Fig. 3.5.11. The growth system with no source, and the applied temperature profile (after Nakajima et al. [2002]).

implying that 0.3 mm/h was the optimum pulling rate. Indeed, the measured *Si* composition along the growth direction, by EDX, verifies that the pulling rate of 0.3 mm/h leads to the most uniform crystal (Fig. 3.5.10b). The section with the uniform composition is about 5.5 mm, after which large fluctuations in the composition are observed.

Azuma et al. [2001] gave an explanation for the dynamics of the growth rate observed in the MCZM growth of  $Si_xGe_{1-x}$  (see Fig. 5.3.9a, as we will see in the next section, this concept led to the utilization of the LPD technique by Yildiz et al. [2005]). Under the assumption of a *diffusion limited* growth mechanism, the concept is as follows.

The amount of *Si* species incorporated into the crystal is expressed as

$$J_{Si} = D_C \frac{\partial C_L}{\partial z} + V^g C_L \quad (3.5.1)$$

where  $J_{Si}$  represents the amount of *Si* atoms (mass flux) incorporated into the crystal through the growth interface per unit area and per unit time,  $D_C$  is the diffusion coefficient of *Si* in the solution,  $C_L$  is the number of *Si* atoms per unit volume in the solution, and  $V^g$  is the growth rate. The growth rate is defined by

$$V^g = \frac{J_{Si}}{x_s(T)} \frac{a_{SiGe}^3}{8} \quad (3.5.2)$$

where  $x_s(T)$  is the Si composition in the grown crystal,  $a_{SiGe}$  is the lattice constant of  $SiGe$ , and 8 is the number of atoms in a lattice. By substituting Eq. (3.5.1) in Eq. (3.5.2), and defining  $A \equiv a_{SiGe}^3 / 8$ , we obtain

$$V^g = \frac{D_C A}{x_s(T) + AC_L} \frac{\partial C_L}{\partial z} \quad (3.5.3)$$

where the crystal composition  $x_s(T)$  increases with the increasing temperature at the interface while the change in  $\partial C_L / \partial z$  would be comparatively small. Hence, at the early stages of the growth process, since the liquid solution is still rich in *Si*, a relatively small amount of *Si* is needed from the source. The availability of *Si* in the solution leads to a fast growth initially. However, later, due to the depletion of *Si* in the solution during growth, the crystallization at the interface will be delayed until the dissolved *Si* species reach the growth interface. This naturally slows down the growth process as the growth progresses (see Azuma et al. [2001] for details).

## *Growth of $Si_xGe_{1-x}$ from the Si-rich Side*

The MCZM technique was extended by Nakajima et al. [2002] for the growth of  $Si_xGe_{1-x}$  single crystals on  $Si$  from the  $Si$ -rich side of the phase diagram. Two growth systems have been used; one without the supply of solute, and the other one with a source system to supply  $Si$  to the solution continuously. The growth systems are shown in Figs. 3.5.11 and 3.5.12.

In the system shown in Fig. 3.5.11, used for the growth of *SiGe* on *Si*, the temperature furnace profile was selected to have a uniform zone at the higher temperature region (the lower region) and a lower temperature section at the

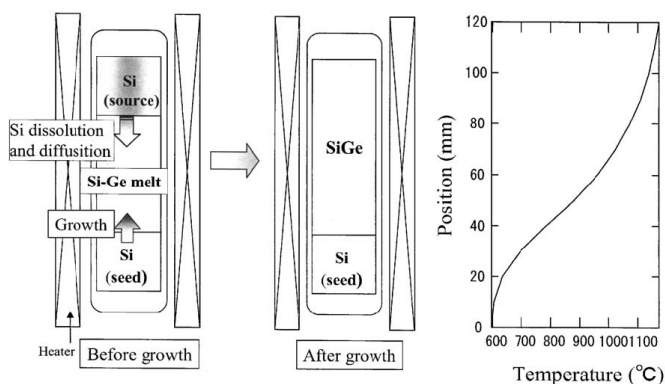


Fig. 3.5.12. Growth system with source, and the applied temperature profile (after Nakajima et al. [2002]).

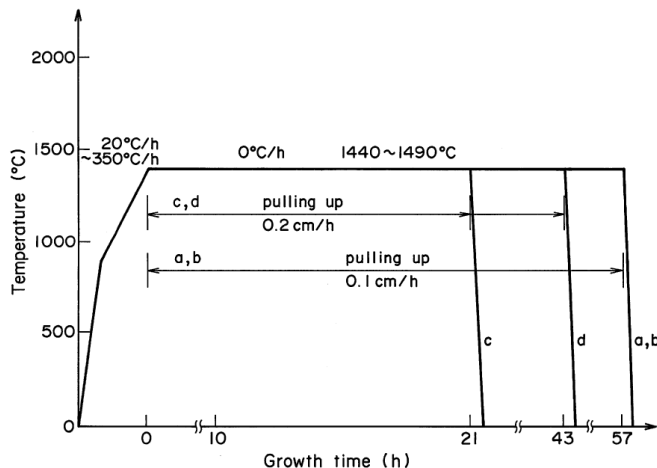


Fig. 3.5.13. Furnace temperature as a function of growth time for the growth of *Si*-rich *SiGe* bulk crystals using the apparatus with no source (after Nakajima et al. [2002]).

upper region with a proper gradient. The single crystal (100)*Si* is 1.5-cm and the (100)*Ge* crystal is 1.0-cm long, both with a diameter of 1.5 cm. The *Si* and *Ge* crystals were undoped, and were of purity of  $\sim$ 10 nines. The inner diameters of the quartz and carbon crucibles are 1.5 cm and 1.7 cm, respectively. The crucible was rotated at 0.5 and 1.0 rpm. After the application of the thermal profile, the liquid zone was allowed to become a fully-mixed solution of *Si*-*Ge*. Then, the crucible is pulled upward. As the growth progresses, the *Si* concentration in the solution decreases gradually. In this system, the *Si* crystal plays the role of both the source and the seed. The furnace temperature program is shown in Fig. 3.5.13 (see Nakajima et al. [2002] for details).

In the growth system shown in Fig. 3.5.12, the temperature profile has a uniform zone and a rapidly cooling zone with a large temperature gradient. It is designed to grow *SiGe* on a *Si* seed with the supply of *Si* into the solution from a *Si* source. A (100) *Si* single seed crystal of 1.0 cm in length, a *Ge* crystal of 2.0 cm, and the (100) *Si* single crystal source of 1.0 cm were stacked in the 1.5 cm quartz crucible, and sealed in high vacuum. The crucible was rotated at 1.0 rpm. The system was rapidly heated up to 1180°C. The locations of the *Si* and *Ge* crystals were determined to set the interface temperature at 1100°C. At this arrangement, the *Ge* crystal melts completely, and the seed and the source crystals melt partially. The initial solution composition was determined from equilibrium at the interface temperature of 1100°C. The crucible was kept stationary at its initial position during growth. The growth process was terminated by rapid cooling after a growth time of about 100 h.

The *Ge* composition profiles of the *SiGe* crystals grown without source are presented in Figs. 3.5.14 as a function of the crystal length with respect to the initial seed surface. Results show that the composition profiles of the crystals

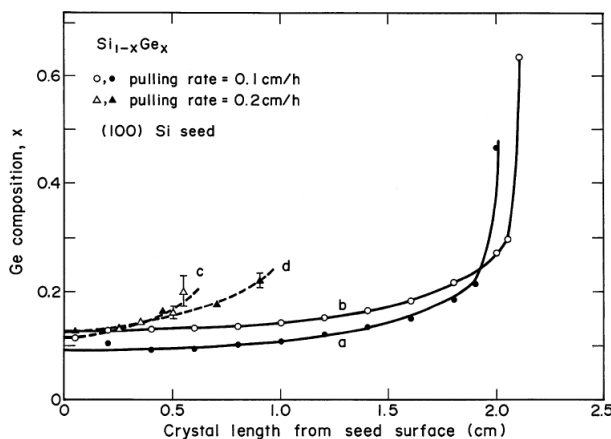


Fig. 3.5.14. Ge composition profiles in the  $Si$ -rich  $SiGe$  bulk crystals, grown without source (after Nakajima et al. [2001]).

grown at the 0.1 cm/h pulling rate are more uniform than those grown at 0.2 cm/h. This shows that the pulling rate of 0.1 cm/h was optimum, at which the growth temperature remains almost constant during growth. This is because the position of the growing interface was kept fixed with respect to the temperature profile of the furnace. With these experiments, it was possible to grow 1.5-cm long  $Si$ -rich  $Si_{1-x}Ge_x$  bulk crystals with a uniform composition of  $x = 0.1$ , without using any supply mechanism. As expected, the  $Ge$  composition sharply increases at the end of the crystals due to the depletion of  $Si$  in the solution.

As seen in Fig. 3.5.15a, the initial  $Ge$  composition is about 0.5 as dictated by the equilibrium condition at the interface temperature of 1100°C. In comparison with that in the  $Ge$ -rich system, the initial composition in the  $Si$ -rich system can easily be determined by simply controlling the growth temperature. This is because the  $Si$  seed stays in the solid form at the growth temperature while the  $Ge$  seed crystal melts down (Nakajima et al. [1999], Azuma et al. [2001]). The  $Ge$  composition decreases as the growth interface approaches the  $Si$  source and the growth temperature becomes continuously higher. The supply of  $Si$  is very effective in changing the compositional variation in the  $Si$ -rich  $SiGe$  crystals. Fig. 3.5.15b shows the position of the growth interface as a function of growth time, measured using an in-situ monitoring system (Azuma et al. [2001]). After an initial 8 h growth period, the growth rate remains almost constant. The growth rate was about 0.2 cm/h.

The  $Ge$  composition profiles, measured along the radial direction (at distances between 0.05 cm and 0.55 cm from the  $Si$  seed), are shown in Fig. 3.5.16. The composition is very uniform in the sections near the seed, but it becomes  $Ge$ -rich near the end. This implies that the shape of the growing interface becomes

convex as growth progresses (this will be discussed further in the next section, in the LPD growth of  $SiGe$ ).

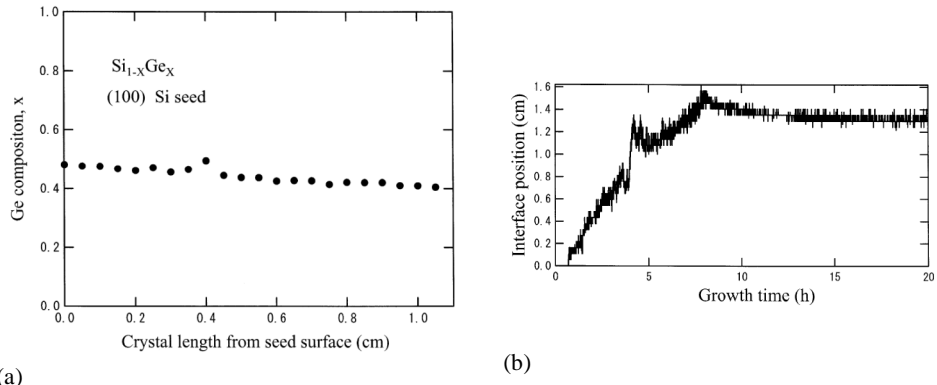


Fig. 3.5.15. (a)  $Ge$  composition profile (along the growth direction) in an  $Si$ -rich  $SiGe$  bulk crystal grown with the source system. (b)  $Ge$  composition profile in Crystal d along lines perpendicular to the growth direction, measured on several cross sections at 0.05–0.55 cm away from the  $Si$  seed (after Nakajima et al. [2001]).

As stated in Nakajima et al. [2001], in the MCZM technique with no source, the growth temperature must be kept constant during growth in order to grow  $SiGe$  bulk crystals with uniform compositions (as in the case in Czochralski and Bridgman growth). When the MCZM growth method is provided with a supply mechanism (as in Floating-Zone),  $SiGe$  bulk crystals with uniform compositions can be grown by achieving a precise balance between the growth rate and the

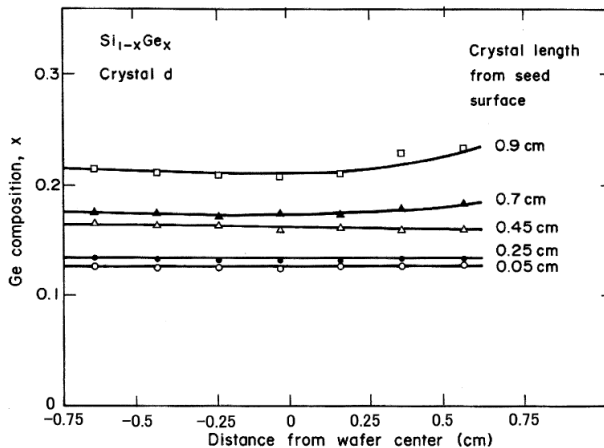


Fig. 3.5.16.  $Ge$  composition along the radial direction (after Nakajima et al. [2001]).

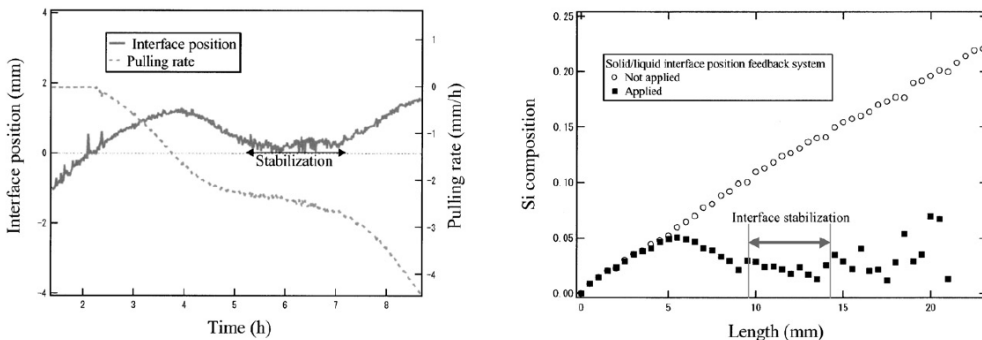


Fig. 3.5.17. (a) Change in the interface position and the pulling rate of the crucible with time (for a 20 mm-long melt). The interface position was stabilized at the indicated period. (b) Comparison of the compositional distribution of *SiGe* bulk crystals grown with and without feedback control (after Azuma et al. [2003]).

pulling rate.

Azuma et al. [2003] developed an automatic feedback control system for the MCZM technique to control the position of the growth interface in order to keep the temperature at the interface constant during growth. It was shown that this system can be used successfully for the growth of *Ge-rich SiGe* bulk crystals with uniform compositions (see Azuma et al. [2003] for details). In this system, the position of the crystal–melt interface is detected using an in-situ monitoring system (capturing images by a CCD camera), and based on the information from the growth interface the crucible pulling rate is then corrected continuously (at every minute). The system was also effective even when the growth rate varied significantly.

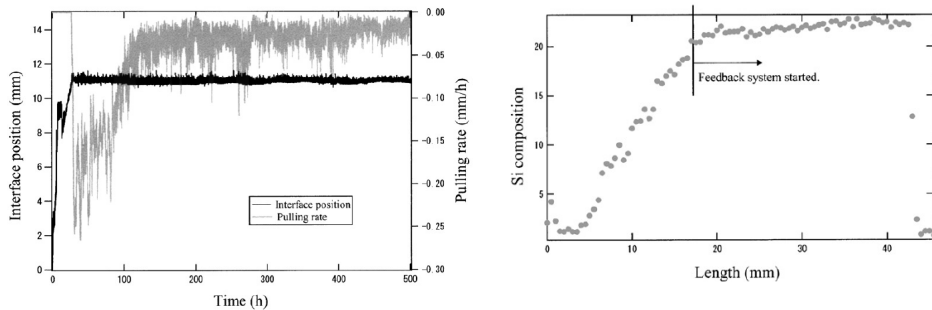


Fig. 3.5.18 (a) Change in the interface position and the pulling rate with time (for a 80 mm-long melt). The feedback control system used keeps the interface position stationary for 470 h during growth. (b) Composition distribution of the *SiGe* crystal (from the 80 mm-long melt) grown with the feedback control system (after Azuma et al. [2003]).

### 3.5.3. Liquid Phase Diffusion Growth of $Si_xGe_{1-x}$

As discussed in the previous section, the growth mechanism of the MCZM technique was explained by assuming a diffusion limited growth process. Although there may be other effects such as kinetics, convection, etc., to be included, the assumption of diffusion limited was a close and simple one. Based on this idea of Nakajima et al. [1999], Yildiz et al. [2005] utilized the MCZM technique for the growth of  $Si_xGe_{1-x}$  crystals on  $Ge$  (from the  $Ge$ -side). The growth technique was called liquid phase diffusion to reflect the fact that in the growth of  $Si_xGe_{1-x}$  by MCZM, the growth *melt* is actually a binary liquid solution of  $Si$ - $Ge$  which is formed from a  $Ge$  melt by dissolving  $Si$  into it. In this sense, the LPD system used by Yildiz et al. [2005] is a *solution* growth technique similar to THM, not to the zone-melting techniques.

The LPD growth system developed and used to grow  $Ge$ -rich  $Si_xGe_{1-x}$  bulk single crystals with axially varying silicon composition is shown schematically in Fig. 3.5.19. For the growth experiments, a three-zone solid tubular furnace capable of operation at temperatures up to  $1250\ ^\circ C$  was utilized. The temperature of each zone is independently controllable. The outer quartz ampoule (growth reactor) is used as an envelope for the growth cell. The inner quartz ampoule is used as a crucible and serves three main purposes; first, it prevents spilling of growth material into the furnace in case the quartz ampoule breaks; second, it facilitates the loading process of the growth charge into the ampoule; third, it creates spaces for the deposition of volatile reaction products

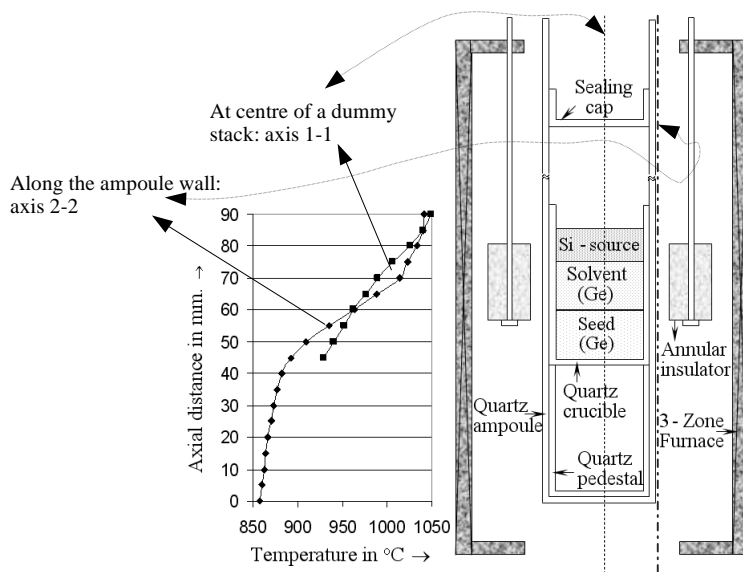


Fig. 3.5.19. LPD growth system and the applied temperature profile (after Yildiz et al. [2005]).

such as  $SiO$ , which is mainly formed due to the reaction between the silicon and quartz crucible walls as well as residual oxidizing atmosphere. At the bottom of the crucible is an annular quartz pedestal used to move the growth cell up and down inside the ampoule during the determination of the axial temperature profile since the quartz ampoule is stationary. The quartz crucible contains three layers of vertically stacked charge materials, namely single crystal germanium as a substrate with (111) crystallographic orientation, germanium blocks or chunks to form a liquid solvent, and finally polycrystalline silicon as a source material. The growth domain is of 40 mm height and 25 mm diameter. The charge materials are core-drilled from Cz-grown boules and polycrystalline silicon bar (for the  $Ge$ -substrate and the  $Si$ -source, respectively) using a diamond impregnated core drill to a diameter slightly larger than the inner diameter of the quartz crucible.

Before loading the growth charge into the growth cell, all quartz parts are etched for 15 minutes in diluted (10%) hydrofluoric acid and then rinsed with deionized water (18 MΩ resistivity) and dried with methanol. The charge materials are chemically etched in a mixture of HF (49 %):HNO<sub>3</sub> (68-70%) with the ratio of 1:3 to remove surface oxides and to fit their diameter to the quartz crucible. Having loaded the quartz pedestal and the crucible hosting the growth charge into the quartz ampoule, the quartz ampoule is evacuated using a turbo molecular pump and then flushed with high purity hydrogen several times to remove oxidizing atmosphere. Finally, it is evacuated to a pressure of approximately  $5 \times 10^{-3}$  Pa and sealed under this pressure by a quartz sealing cap. The quartz sealing cap is held suspended inside the ampoule with a quartz hook during the evacuation and sealing process.

A well-determined, steep and stable temperature profile is required in LPD for two reasons. The first is to be able to obtain large solute composition gradient in a grown crystal, and the second is to prevent the total melting down of the germanium substrate, which is the main difficulty of growing  $Si_xGe_{1-x}$  on  $Ge$ . Therefore, prior to growth trials, several temperature profile measurements were taken to determine the best-possible location for the growth crucible within the outer quartz tube as well as to find appropriate temperatures for each zone of the furnace. To achieve a steep thermal gradient in the region of the growth charge, an annular ceramic insulator material is placed around the quartz ampoule and covers the tube starting slightly above the substrate up to the middle of the source. The ceramic insulator is suspended in the middle zone of the furnace with a pair of T-shaped quartz rods which are attached to a flange assembly located at the top of the furnace. A thermocouple is inserted into the furnace through the upper flange assembly to monitor the thermal stability of the growth process. The temperature profile in the quartz crucible was measured using a center drilled silicon dummy block. The temperature gradient measured within the growth region was approximately 23°C/cm inside the crucible and 40°C/cm on the outside wall of the quartz ampoule.

### Growth of $Si_xGe_{1-x}$ Single Crystals by LPD

During the growth process, the quartz ampoule is held stationary and placed in an appropriate temperature gradient (Fig. 3.5.19). The growth process is initiated by firing the furnace to reach a predetermined temperature profile at an appropriate rate. Then, this temperature profile is kept constant throughout the growth. The growth procedure is as follows.

The furnace temperature is first raised up to a point approximately 60°C lower than the real growth temperature (at which the germanium charges are still solid) at a rate of ~155°C/h and then kept at this temperature until the temperature profile is stabilized. Thereafter, the system is heated up to the selected growth temperature profile within 2.5 hours. When the temperature around the growth cell reaches the growth temperature, the polycrystalline germanium melts completely and forms the growth solvent. The single crystal germanium substrate melts partially, down to a thickness of about 8-10 mm. The silicon source material remains solid due to its higher melting temperature. At the growth temperature, according to the *Si-Ge* binary phase diagram, the silicon source begins to dissolve into the germanium melt, depending on the temperature across the dissolution interface. Thus, the *Si-Ge* growth solution begins to form. The dissolved silicon species (solute) moves in the growth solution towards the growth interface.

The growth mechanism of LPD can best be visualized by considering the equilibrium phase diagram of the *Si-Ge* system. A sketch of the growth cell is presented in Fig. 3.5.20, along with the germanium rich section of the representative binary phase diagram of *Si-Ge*. The transport of silicon species (solute) towards the growth interface enhances the solute concentration in the vicinity of the growth interface, and makes the solution near the interface supersaturated at  $x_1^L$ , and consequently supercooled at  $T_1^L$ . Naturally,  $T_1^L$  is higher than the liquid temperature in the vicinity of the interface, indicated by a dashed line in the figure, and the supersaturated solution solidifies at the silicon composition of  $x_1^S$ . The growth interface then moves to a new position. The silicon composition in the solid (Constitutionally Super-cooled Liquid, CSCL)  $x_1^S$  is higher than that in the supersaturated solution, leading to an increase in the germanium concentration near the growth interface due to the rejection of germanium species into the liquid. As a result, the liquidus (equilibrium) temperature of the solution at the interface drops below the liquid temperature. The transport of silicon species towards the growth interface supersaturates the solution near the interface, and leads to crystallization. This process repeats itself, and the growth is maintained by the constitutional supercooling of the solution at the interface due to the continuous supply of silicon species into the solution. Throughout the growth process, unremitting silicon depletion in the solution is compensated by continuous supply of silicon species from the top-located silicon feed. As the growth progresses, the growing interface moves up, leading to an increase in the growth temperature and in turn the silicon

concentration at the interface. The above-discussed LPD growth configuration allows the growth of compositionally graded  $Si_xGe_{1-x}$  single bulk crystals with an increasing silicon composition along the growth direction. The growth process is terminated when the entire solution solidifies completely. The furnace is first cooled at a rate of  $15\text{ }^{\circ}\text{C/h}$  from the growth temperature to just below the melting temperature of pure germanium to prevent crack generation due to the thermal shock in the solidified crystal and the quartz crucible, and then in the furnace atmosphere down to room temperature. The total growth time used in the present study is 96-120 hours.

As we will see in Chapter 8, the numerical simulation model developed to study the transport phenomena occurring during the LPD growth process in Yildiz and Dost [2005] indeed supports the above interpretations. Simulation results show that the contribution of the buoyancy-induced (thermosolutal) convection is very significant at the early stages of the growth process. However, as the growth progresses, convection gradually weakens with the continuous incorporation of dissolved silicon species into the solution. After a few hours of growth time, convection becomes numerically undetectable, and during the rest of the growth process, silicon is transported towards the growth interface mainly by diffusion.

Pictures of typical sample crystals grown by LPD are shown in Figs.3.5.21 One of the main difficulties of growing  $Si_xGe_{1-x}$  with a germanium substrate is to prevent the substrate from being totally melted. It requires a number of

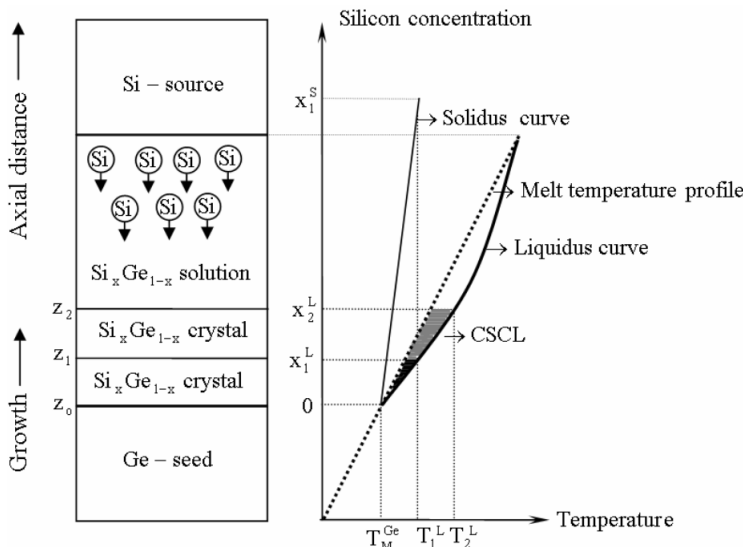


Fig. 3.5.20. A representative diagram for the growth mechanism of LPD growth technique (after Yildiz et al. [2005]).

experiments to obtain appropriate temperatures for each zone of the furnace since visual access to the growth zone is not possible. A number of compositionally graded, fully and partially single  $Si_xGe_{1-x}$  crystals were grown.

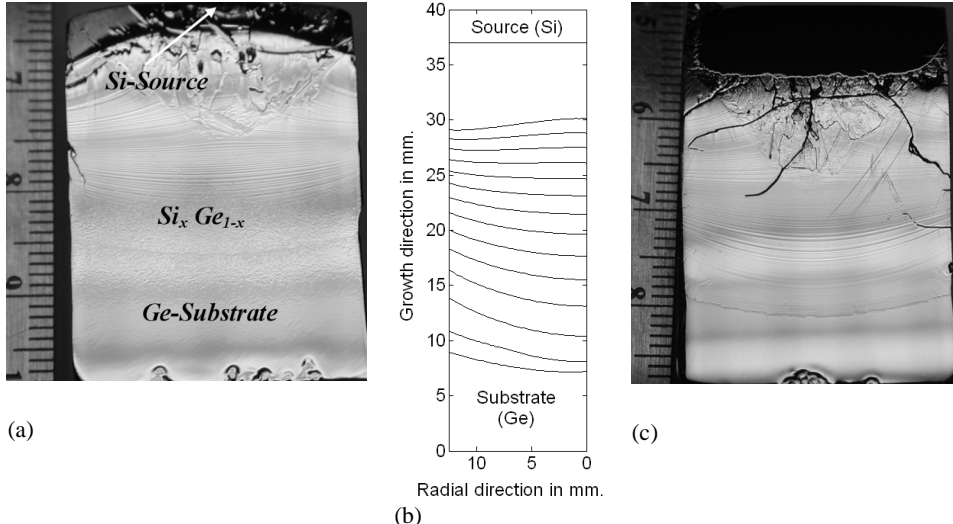


Fig. 3.5.21. Two samples of the LPD grown compositionally graded  $Si_xGe_{1-x}$  single crystals (a) and (c), and evolution of the computed interfaces (b) (the time interval between each line is three hours, and total simulated growth time is 39 hours). The agreement between experimental (c) and simulation results (b) are quite good (Yildiz et al. [2006b] and Yildiz and Dost [2005]).

The diameter and the length of the grown  $Si_xGe_{1-x}$  crystals are 25 mm and between 20 and 25 mm, respectively. For compositional analysis and delineation of single crystallinity, the grown crystals were bisected along the growth axis. A 2-mm thick plate was cut off from the first half to determine axial and radial composition distributions of Si. The cut and polished samples were used to determine the compositions of the grown single crystals. The measurements were made at various axial and radial locations by Electron Probe Microanalysis (EPMA) and EDX with the acceleration voltage of 20 kV and SiK 1.739 keV and GeK 9.873 keV peaks.

All the crystals grown using 10 mm thick silicon source materials involve extensive amount of cracks in the close vicinity of the dissolution interface. The cracks penetrate into the crystal body to a certain extent. The cracks have been generated possibly because of the mismatch in the thermal expansion coefficients between the undissolved silicon source and the  $Si_xGe_{1-x}$  solid solution. There might be a possible contribution of large lattice mismatch (approximately 4.2%) between the silicon source and the  $Si_xGe_{1-x}$  crystal. In order to eliminate such cracks, growth experiments were later carried out using silicon sources thin enough (2-3 mm) to ensure that after the growth, the silicon

sources are entirely dissolved or little left over. It was observed that cracks emanated from the remaining silicon source and the silicon source free regions did not show any sign of cracks (see sample in Fig. 3.5.21c).

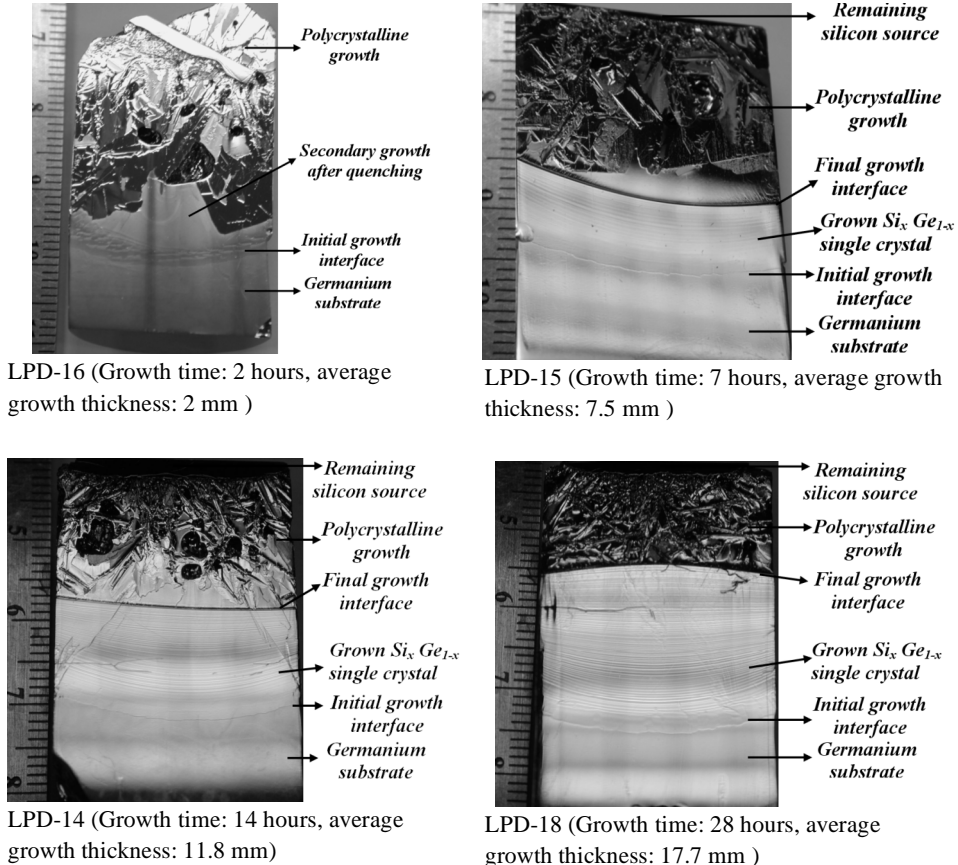


Fig. 3.5.22. Sample LPD grown crystals for interface evolution (Yildiz et al. [2006b]).

In all the grown crystals, the interface shape is initially concave with approximately a 1.5-2.0-mm curvature depth. The steepness of the interface depends on the remaining thickness of the substrate as well. The larger the remaining thickness, the shallower the growth interface since the thicker substrate facilities heat transfer in the axial direction. The development of the initial concave shape can be attributed to (i) the large variations between the thermal conductivities of the substrate, grown crystal, and the quartz crucible, and also (ii) the presence of an insulating section in the design to achieve the intended steep temperature profile as mentioned earlier. The concave interface shape implies that heat loss from the periphery of the crucible is larger than that

from the bottom. Therefore, it is possible to control the interface shape by changing the heat transfer characteristics of the system.

All crystals show a high degree of single crystallinity up to 6-8 % at.Si. This implies that it is possible to extract  $Si_xGe_{1-x}$  single crystal substrates from the region which offers the specific composition of interest.

### *Interface Evolution*

As can be seen from Figs. 3.5.21a,c, the initially concave growth interface gradually becomes flatter as the interface moves up. In the middle region, the interface is almost flat and then becomes convex as it approaches the source material. This change in the curvature of the growth interface is due to the change in the temperature field in the solution as growth progresses. The temperature field changes mainly because of the effect of the annular ceramic insulator on the thermal profile as well as because of the increase in the thickness of the solid region.

To calculate the rate of the growth interface movement (the growth velocity,  $V^g$ ), and also to examine the evolution of the growth interface, four growth experiments were devised (Fig. 3.5.22). Each growth experiment was terminated after a certain time period by switching off the furnace so that the growth zone is quenched within the furnace atmosphere. Then, by observing the interface between the single and polycrystalline regions, the average thickness of the grown crystal is determined. The interface positions were measured at two locations, the center and the edge points, in the grown crystals, and are plotted in Fig. 3.5.23. As can be seen, the growth velocity is not uniform along the interface, and also not constant along the growth direction. For the growth interface to become flatter, and later convex, as the crystal grows, the central region of the crystal has to grow faster than the edges. The variation of the growth velocity in the radial direction may be explained as follows.

As the growth proceeds, the initially isothermal growth interface becomes non-isothermal due to the transient nature (non-equilibrium) of the growth process. This leads to variations in the local saturations, and in turn varies the growth velocity across the interface. As for the variation along the growth direction, one may consider the species mass balance at the growth interface, i.e.,

$$V^g = \frac{\rho_L D_{Si}^L}{\rho_s (c_{gi}^s - c_{gi}^L)} \frac{\partial c}{\partial n} \quad (3.5.4)$$

where  $c_{gi}^s$  and  $c_{gi}^L$  are the equilibrium mass fractions of silicon in the solution and the solidified crystal at the interface, obtained from the  $Si-Ge$  binary phase diagram. From the phase diagram, one can see that the term  $(c_{gi}^s - c_{gi}^L)$  increases due to an increase in interface temperature as the growth interface moves. Given that the concentration gradient along the growth direction remains nearly

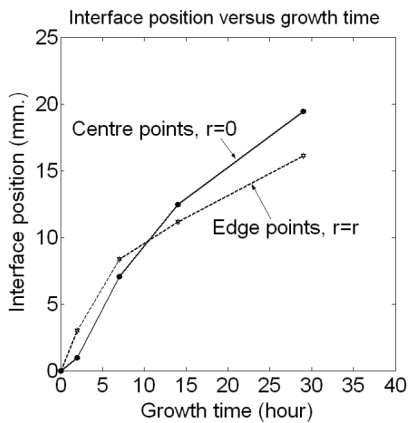


Fig. 3.5.23. Interface displacement versus growth time for the center and edge regions of the grown crystals (after Yildiz et al. [2005], [2006b]).

constant during the growth process, the growth velocity should be inversely proportional to the term  $(c_{gi}^s - c_{gi}^L)$ . Thus, the growth velocity has to decrease as the growth interface travels to the higher temperature regions. This solely mathematical evaluation implies that at the beginning of the growth, a lesser amount of silicon atoms is needed to saturate the interface for solidification. However, as the growth interface moves to the higher temperature regions, more silicon atoms are needed for supersaturation so that the growth velocity is expected to be not as fast as before. Thus, the growth velocity decreases as the growth progresses. It is also noted the variation in the growth velocity is not linear.

#### Growth Striations

Growth striations were observed in all the crystals grown by LPD in Yildiz et al. [2005, 2006b]. The occurrence of growth striations is known in crystals grown by the techniques (e.g., Czochralski and Bridgman) involving intentional mechanical movements such as pulling, rotation, or translation, and their occurrence can be attributed to the disturbance caused by such mechanical movements. Growth striations were, however, not expected in the LPD grown crystals since there is no mechanical movement of any kind in the present set up. To the best of our knowledge, no striations were reported in the literature in the MCZM of *SiGe* crystals.

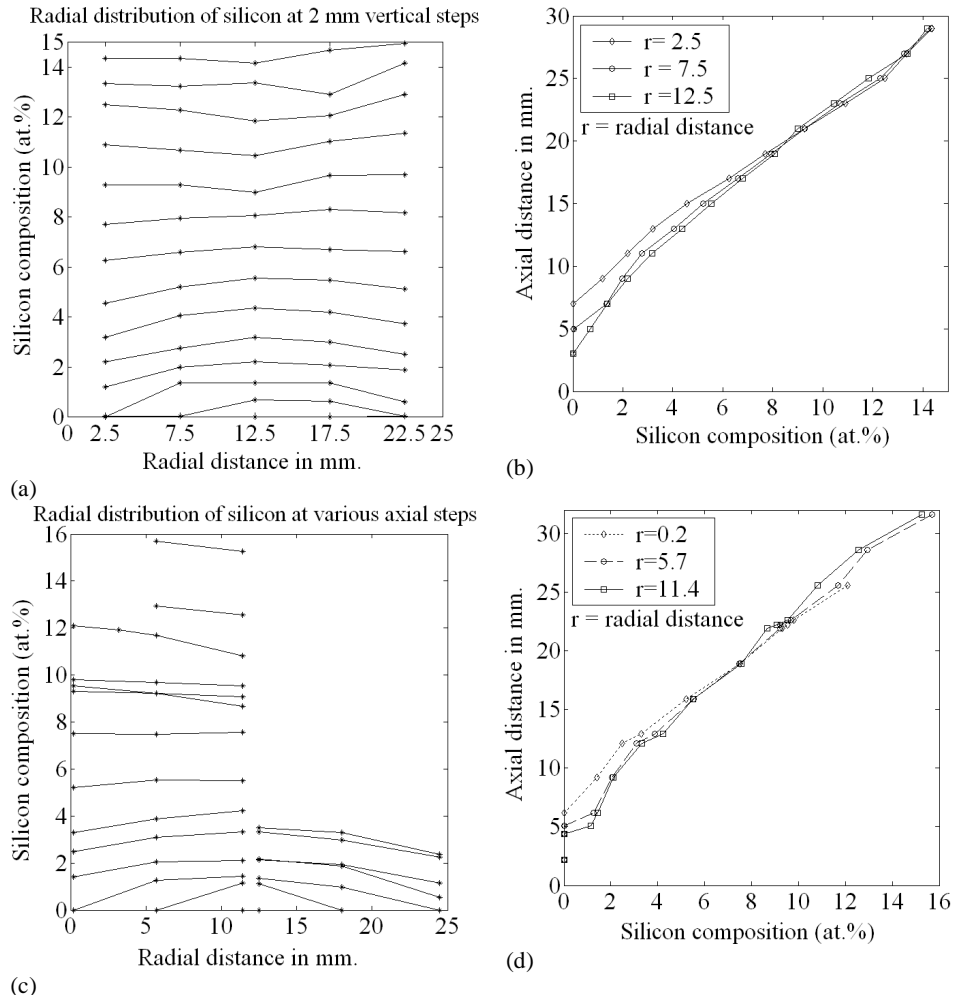


Fig. 3.5.24. Silicon concentration distribution in LPD grown *SiGe* crystals: with EPMA (a) in the radial direction (at 2 mm vertical steps), (b) in the axial direction, and with EDX (c) in the radial direction (at various vertical steps) and (d) in the axial direction (after Yildiz et al. [2005]).

Nevertheless, the presence of such striation lines in the LPD grown crystals was extremely beneficial to the modeling study of Yildiz and Dost [2005] in terms of comparing the evolution of the numerically computed growth interfaces with experiments. As can be seen from Fig. 3.5.21b,c, the striation lines in the crystals closely follow the computed shapes of the evolving growth interface (for the half geometrical domain is shown on the left, time interval between each line is three hours, and the total simulated growth time is 39 hours. A cross section of an LPD grown crystal is shown on the right. The

agreement between experimental and simulation results is quite good (details of the numerical modeling will be discussed in Chapter 8).

As mentioned earlier there are no external reasons for the presence of growth striations in our crystals. However, one may think of three possible contributing sources: i) the continuous change in the temperature field during growth, ii) the convection in the liquid zone, and iii) the constitutional supercooling near the growth interface. As mentioned earlier, the continuous change in the temperature field is due to the thermal character of the growth crucible, and may contribute to the fluctuations in the concentration field. Secondly, since the convection is very strong at the beginning, although it gets weaker as the growth progresses, it may also cause continuous temperature fluctuations leading to concentration fluctuations in the solution. Finally, during the growth process, silicon is preferentially consumed at the growth front. This may, although very small, further contribute to the fluctuations in the concentration field. These fluctuations in the concentration field might consequently have led to growth striations in the grown crystals.

It is noted that the spacing between striation lines is wider at the early stages of the growth (when the growth velocity is faster, and the convection is stronger), and it gets narrower as the growth interface moves closer to the source material (when the growth velocity is slower, and the convection is weaker).

### *Silicon Composition*

Figs. 3.5.24 present the silicon composition distribution along both the axial and radial directions, measured respectively by EPMA and EDX. The characterization results from the same crystals performed with two techniques are very close. As expected, the silicon concentration increases along the growth direction, and exhibits a relationship close to a linear variation in time. The silicon concentration varies slightly in the radial direction, following very closely the evolution of the growth interface. As the growth interfaces get flatter (Fig. 3.5.21), the radial silicon distribution follows the same trend. Figs. 3.5.24 also provide information on the evolution of the growth interface since the radial concentration distribution can be considered closely related to the isotherms in the liquid near the growth interface. The region with a homogeneous radial concentration distribution offers the possibility of extracting wafers to be used as seeds.